

## **CCL5 promotes breast cancer recurrence through macrophage recruitment in residual tumors**

Andrea Walens, Ashley V. DiMarco, Ryan Lupo, Benjamin R. Kroger, Jeffrey S. Damrauer, and James V. Alvarez

Department of Pharmacology and Cancer Biology, Duke University, Durham, NC 27710, USA

Keywords: breast cancer, CCL5, macrophage, collagen

The authors declare that they have no conflict of interest relevant to this work.

1 **ABSTRACT**

2 Over half of breast cancer related deaths are due to recurrence five or more years after initial  
3 diagnosis and treatment. This latency suggests that a population of residual tumor cells can survive  
4 treatment and persist in a dormant state for many years. The role of the microenvironment in  
5 regulating the survival and proliferation of residual cells following therapy remains unexplored.  
6 Using a conditional mouse model for Her2-driven breast cancer, we identify interactions between  
7 residual tumor cells and their microenvironment as critical for promoting tumor recurrence. Her2  
8 downregulation leads to an inflammatory program driven by TNF $\alpha$ /NF $\kappa$ B signaling, which  
9 promotes immune cell infiltration in regressing and residual tumors. The cytokine CCL5 is  
10 elevated following Her2 downregulation and remains high in residual tumors. CCL5 promotes  
11 tumor recurrence by recruiting CCR5-expressing macrophages, which may contribute to collagen  
12 deposition in residual tumors. Blocking this TNF $\alpha$ -CCL5-macrophage axis may be efficacious in  
13 preventing breast cancer recurrence.

14

15

## 16 INTRODUCTION

17 In 2018 it is estimated that approximately 270,000 women will be diagnosed with breast  
18 cancer, and 41,000 women will succumb to the disease (Siegel et al. 2018). Historically, over half  
19 of these deaths are due to recurrence 5 or more years after initial diagnosis and treatment (Sosa et  
20 al. 2014). This suggests that in a subset of patients, there is a population of clinically undetectable  
21 residual tumor cells that survive therapy, and may serve as a reservoir for eventual relapse. The  
22 long latency of recurrence has led to speculation that residual tumor cells are slowly growing or  
23 even dormant (Hölzel et al., 2010; Klein, 2009). Understanding how residual cells survive therapy,  
24 persist in a non-proliferative state, and eventually resume proliferation to form recurrent tumors is  
25 critical for preventing recurrences.

26 Much of the work examining mechanisms of tumor cell survival and recurrence following  
27 therapy has focused on tumor cell-intrinsic pathways (Sosa et al., 2011). Genetic mutations that  
28 render cells resistant to therapy represent an important mechanism of survival (Holohan et al.,  
29 2013), but there is emerging evidence that non-genetic pathways can also promote survival in  
30 response to therapy. For instance, a population of cells called drug-tolerant persisters has been  
31 shown to survive therapy through epigenetic adaptations (Sharma et al., 2010). Additionally,  
32 epithelial-to-mesenchymal transition has been shown to promote cell survival in response to EGFR  
33 inhibitors (Sequist et al., 2011). Finally, alterations in apoptotic pathways within tumor cells can  
34 promote cell survival in response to both chemotherapy and targeted therapy (Alvarez et al., 2013;  
35 Damrauer et al., 2018; Hata et al., 2016; Holohan et al., 2013; Mabe et al., 2018). In spite of this  
36 extensive literature on cell-intrinsic mechanisms of therapeutic resistance, much less is known  
37 about tumor cell-extrinsic contributions to cell survival following therapy. Specifically, while there  
38 has been some recent focus on how the tumor microenvironment can promote tumor cell survival

39 in response to therapy (Meads et al., 2009), little is known about whether the microenvironment  
40 regulates tumor cell survival, dormancy, and eventual recurrence.

41 We used a conditional mouse model of Her2-driven breast cancer to examine interactions  
42 between tumor cells and their microenvironment during tumor dormancy and recurrence. In this  
43 model, administration of doxycycline (dox) to bitransgenic MMTV-rtTA;TetO-Her2/neu  
44 (MTB;TAN) mice leads to mammary gland-specific expression of epidermal growth factor  
45 receptor 2 (Her2) and the development of Her2-driven tumors. Removal of dox induces Her2  
46 downregulation and tumor regression. However, a small population of residual tumor cells can  
47 survive and persist in a non-proliferative state (Alvarez et al., 2013; Moody, 2002). These cells  
48 eventually re-initiate proliferation to form recurrent tumors that are independent of Her2. Using  
49 this model, we sought to understand how the interplay between tumor cells and their  
50 microenvironment regulates residual cell survival and recurrence.

51

## 52 RESULTS

### 53 **Her2 downregulation induces an inflammatory gene expression program driven by the** 54 **TNF $\alpha$ /IKK pathway**

55 To understand how interactions between tumor cells and their environment change in  
56 response to therapy, we first examined gene expression changes following Her2 downregulation  
57 in Her2-driven tumor cells. Two independent cell lines derived from primary Her2-driven tumors  
58 (Alvarez et al., 2013; Moody, 2002) were cultured in the presence of dox to maintain Her2  
59 expression, or removed from dox for 2 days to turn off Her2 expression. Changes in Her2  
60 expression following dox withdrawal were confirmed by qPCR analysis (Figure 1 – figure  
61 supplement 1A). Changes in gene expression were measured by RNA sequencing. Her2  
62 downregulation led to widespread changes in gene expression in both cell lines (Figure 1A). Gene  
63 set enrichment analysis showed that an E2F signature was the most highly enriched gene set in  
64 cells with Her2 signaling on (+dox; Figure 1 – figure supplement 1B), consistent with previous  
65 literature and the observation that Her2 is required for the proliferation of these cells (Lee et al.,  
66 2000). Interestingly, the gene sets most significantly enriched in cells following Her2  
67 downregulation (-dox) were an inflammatory gene signature and a TNF $\alpha$ /NF $\kappa$ B gene signature  
68 (Figure 1B). These gene sets comprised genes encoding chemokines in the CCL family (CCL2,  
69 CCL5, and CCL20) and CXCL family (CXCL1, CXCL2, CXCL3, CXCL5, and CXCL10),  
70 proteins that mediate cell-cell interactions (TLR2, ICAM1, and CSF1) as well as signaling  
71 components of the NF $\kappa$ B pathway (NFKBIA and NFKBIE). All of these genes were upregulated  
72 following Her2 downregulation (Figure 1C).

73 At high concentrations (>40  $\mu$ g/ml) doxycycline itself can inhibit the NF $\kappa$ B pathway  
74 (Alexander-Savino et al., 2016; Santa-Cecília et al., 2016). Although the concentrations of dox (2

75  $\mu\text{g/ml}$ ) we use to culture primary tumor cells are well below these levels, we wanted to confirmed  
76 that the NF $\kappa$ B pathway activation observed following dox withdrawal was due to loss of Her2  
77 signaling. To do this, we treated primary tumor cells with Neratinib, a small-molecule inhibitor of  
78 Her2, to inhibit Her2 signaling without removal of dox. Neratinib treatment led to an increase in  
79 phospho-p65 (Figure 1 – figure supplement 1C), increased expression of TNF $\alpha$  (Figure 1 – figure  
80 supplement 1D), and increased expression of the NF $\kappa$ B targets CXCL5 and CCL5 (Figure 1 –  
81 figure supplement 1E and F). To further confirm that the low concentrations of dox used to culture  
82 primary tumor cells do not directly inhibit the NF $\kappa$ B pathway we treated NIH3T3 cells with TNF $\alpha$   
83 in the presence or absence of 2  $\mu\text{g/ml}$  dox and measured NF $\kappa$ B target genes. Dox treatment had  
84 no effect on the induction of NF $\kappa$ B target genes following TNF $\alpha$  treatment (Figure 1 – figure  
85 supplement 1G). Taken together, these results demonstrate that Her2 inhibition leads to activation  
86 of the NF $\kappa$ B pathway.

87         Given the coordinated upregulation of these NF $\kappa$ B target genes, we reasoned that their  
88 expression may be induced by a common upstream secreted factor acting in an autocrine manner.  
89 To test this, we collected conditioned media from primary tumor cells grown in the absence of dox  
90 for 2 days. This conditioned media was supplemented with dox to maintain Her2 expression and  
91 added to naïve primary tumor cells. Treatment with conditioned media led to a time-dependent  
92 upregulation of the pro-inflammatory chemokine CCL5 (Figure 1D). One common upstream  
93 mediator of this cytokine response is tumor necrosis factor alpha (TNF $\alpha$ ), and we found that TNF $\alpha$   
94 expression is increased between 10-fold and 100-fold following Her2 downregulation (Figure 1E).  
95 To test whether this is sufficient to activate downstream signaling pathways, we examined  
96 activation of the NF $\kappa$ B pathway following treatment with conditioned media from cells following  
97 Her2 downregulation. Indeed, we found that treatment of naïve cells with Her2-off (–dox)

98 conditioned media led to rapid, robust, and prolonged activation of the NF $\kappa$ B pathway as assessed  
99 by phosphorylation of p65 (Figure 1F). Importantly, Her2 levels remained high in these target cells  
100 (Figure 1 – figure supplement 1H), indicating that Her2-off (–dox) conditioned media can activate  
101 the NF $\kappa$ B pathway even in the presence of Her2 signaling. In contrast, conditioned media from  
102 Her2-on (+dox) cells had no effect on p65 phosphorylation (Figure 1 – figure supplement 1I).  
103 Finally, we tested whether the induction of chemokine genes following Her2 downregulation was  
104 dependent upon the NF $\kappa$ B pathway by treating cells with the IKK inhibitor, IKK16. We found that  
105 blocking IKK activity blunted the induction of all chemokine genes following dox withdrawal  
106 (Figure 1G). Taken together, these results suggest that Her2 downregulation leads to the induction  
107 of a pro-inflammatory gene expression program, likely driven by autocrine-acting TNF $\alpha$  and  
108 mediated through the IKK-NF $\kappa$ B pathway.

### 109 **Immune cell infiltration during tumor regression and residual disease**

110 Her2 downregulation in Her2-driven tumors *in vivo* induces apoptosis and growth arrest,  
111 ultimately leading to tumor regression (Moody, 2002). However, a small population of tumor cells  
112 can survive Her2 downregulation and persist for up to 6 months before resuming growth to form  
113 recurrent tumors. These residual tumors can be identified histologically (Figure 2A). Many of the  
114 cytokines and chemokines induced shortly after Her2 downregulation function as chemoattractants  
115 for various immune cells (Binnewies et al., 2018; López et al., 2017). This led us to speculate that  
116 Her2 downregulation *in vivo* may promote infiltration of immune cells into the tumor. We  
117 therefore asked whether the immune cell composition of tumors changed during tumor regression  
118 and in residual tumors. CD45 staining showed that leukocyte infiltration increased dramatically  
119 following Her2 downregulation as compared to primary tumors (Figure 2B-C, Figure 2 – figure  
120 supplement 1A). Surprisingly, leukocytes remained high in residual tumors (Figure 2D, Figure 2

121 – figure supplement 1A). Masson’s trichrome staining revealed prominent collagen deposition in  
122 residual tumors (Figure 2D), consistent with a desmoplastic response in residual tumors. Staining  
123 for the macrophage marker F4/80 showed a dramatic increase in macrophage abundance during  
124 tumor regression (Figure 2C, Figure 2 – figure supplement 1A), and macrophage levels remained  
125 elevated in residual tumors (Figure 2D, Figure 2 – figure supplement 1A). CD3 staining showed  
126 increased T cell infiltration in regressing and residual tumors (Figure 2 – figure supplement 1A,B).  
127 Taken together, these results indicate that Her2 downregulation leads to the infiltration of CD45+  
128 leukocytes, and specifically F4/80+ macrophages. Residual tumors contain high numbers of  
129 macrophages and abundant collagen deposition, consistent with a desmoplastic response.

### 130 **Cytokine profiling of residual tumors**

131 Immune cells can influence tumor cell survival and function (Flores-Borja et al., 2016;  
132 Pollard, 2004). The large number of immune cells present in residual tumors suggests that these  
133 cells may function to regulate the behavior of residual tumor cells. To begin to address this, we  
134 sought to identify secreted factors that are expressed in residual tumors. Residual tumor cells in  
135 the autochthonous MTB;TAN model are unlabeled and are diffusely scattered throughout the  
136 mammary gland, precluding their isolation. Therefore, we used an orthotopic model in which  
137 residual tumors can be easily isolated. In this model, primary Her2-driven tumors are digested,  
138 cultured, and infected with GFP. Cells are then injected into the mammary fat pad of recipient  
139 mice on dox to generate an orthotopic primary tumor. Following dox withdrawal, the fluorescently  
140 labeled residual tumors can be easily microdissected (Figure 2 – figure supplement 1C). We first  
141 confirmed that the orthotopic model exhibited similar patterns of immune cell infiltration as the  
142 autochthonous model. Indeed, we found that macrophage staining increased dramatically during



143 tumor regression and in residual tumors (Figure 2 – figure supplement 1D-F), suggesting the  
144 orthotopic model is appropriate for identifying secreted proteins present in these residual tumors.

145 We generated a cohort of orthotopic primary tumors (n=4) and residual tumors at 28 days  
146 (n=6) and 56 days (n=6) following dox withdrawal. Residual tumors were microdissected using a  
147 fluorescent dissecting microscope. We then made protein lysates from all samples and measured  
148 the expression of cytokines and chemokines using antibody-based protein arrays. Four primary  
149 tumors and four 28-day residual tumors were profiled using a commercially available cytokine  
150 array, which measures the expression of 20 secreted factors. We then used a second commercially  
151 available cytokine array, which measures 40 cytokines and chemokines, to measure cytokine  
152 expression in the whole cohort of tumors. This analysis identified 8 cytokines that were  
153 upregulated in residual tumors as compared to primary tumors (Figure 3A; fold change >2, p<0.1,  
154 Figure 3 – source data), including CCL5, osteoprotegerin (OPG), and Vascular cell adhesion  
155 protein 1 (VCAM-1) (Figure 3B). Interestingly, VCAM-1 has been shown to regulate breast cancer  
156 dormancy (Lu et al., 2011), while OPG can regulate the survival of breast cancer cells (Neville-  
157 Webbe et al., 2004).

158 We next asked whether any cytokines were both induced acutely following Her2  
159 downregulation and remained elevated in residual tumors. We found that only two cytokines,  
160 CCL5 and OPG, fulfilled these criteria. Given that OPG has previously been associated with  
161 dormancy, we focused our attention on CCL5. We then wanted to determine if CCL5 expression  
162 was elevated in human residual breast tumors following treatment. We analyzed a gene expression  
163 dataset of residual breast tumors that remain following neoadjuvant targeted therapy. A number of  
164 secreted factors were upregulated in residual tumors as compared to primary tumors, and CCL5  
165 was one of the most significantly upregulated cytokines in this group (Figure 3C-D and Figure 3

166 – figure supplement 1A-M). To confirm these results, we examined an independent gene  
167 expression data set from breast cancer patients treated with neoadjuvant chemotherapy. We found  
168 that CCL5 expression was also increased in residual tumors in this dataset (Figure 3 – figure  
169 supplement 1N). These results suggest that CCL5 upregulation is a common feature of residual  
170 tumors cells that survive both conventional and targeted therapy in mice and humans, suggesting  
171 it may be functionally important in mediating the survival of these cells.

### 172 **CCL5 expression promotes recurrence following Her2 downregulation**

173 We next wanted to directly assess whether CCL5 plays a functional role in regulating  
174 residual cell survival or recurrence. We first used an ELISA to measure CCL5 levels in orthotopic  
175 primary tumors, residual tumors, and recurrent tumors. CCL5 expression was elevated in residual  
176 tumors, confirming results from the cytokine array, and increased further in recurrent tumors  
177 (Figure 4A). We next engineered primary tumor cells to overexpress CCL5 or GFP as a control  
178 (Figure 4B) and used these cells in an orthotopic recurrence assay to test the effect of CCL5  
179 expression on tumor recurrence. Control or CCL5-expressing cells were injected orthotopically  
180 into recipient mice on doxycycline to maintain Her2 expression. Primary tumors formed with  
181 similar kinetics following injection of control and CCL5-expressing cells, indicating that CCL5  
182 expression had no effect on the growth of primary tumors (data not shown). Following primary  
183 tumor formation, mice were removed from dox to induce Her2 downregulation and tumor  
184 regression. Mice with residual tumors were palpated biweekly to monitor the formation of  
185 recurrent tumors. Tumors expressing CCL5 recurred significantly earlier than control tumors,  
186 indicating that CCL5 expression is sufficient to accelerate tumor recurrence (Figure 4C;  $p=0.023$ ;  
187  $HR=2.14$ ).

188 We next asked if tumor-derived CCL5 is necessary for recurrence. To this end, we used  
189 CRISPR-Cas9 to knock out CCL5 in primary tumor cells (Figure 4D), and tested the effect of  
190 CCL5 knockout on recurrence using the orthotopic recurrence assay described above. The growth  
191 of CCL5 knockout tumors was not different from control tumors expressing a non-targeting  
192 sgRNA (data not shown). Mice were removed from dox, and the latency of recurrence between  
193 control and CCL5 knockout tumors was compared. We found that CCL5 knockout had no effect  
194 on the latency of recurrence (Figure 4E). Taken together, these results suggest that CCL5  
195 expression is sufficient to accelerate recurrence, but tumor-derived CCL5 is not necessary for  
196 recurrence following Her2 downregulation.

197

#### 198 **CCL5 promotes macrophage infiltration in residual tumors**

199 CCL5 is a chemoattractant for various cell types, including T cells, B cells, eosinophils,  
200 basophils, neutrophils, macrophages, and fibroblasts (Dembic, 2015; Lacy, 2017; Lee et al., 2017).  
201 We observe an increase in CCL5 levels during tumor regression and in residual tumors that is  
202 concomitant with immune cell infiltration. We therefore reasoned that the effect of CCL5  
203 overexpression on recurrence may be mediated through its ability to recruit one or more of these  
204 cell types to residual lesions and recurrent tumors. CCL5 can signal through multiple receptors,  
205 including CCR1, CCR3, and CCR5, but it predominately acts through CCR5 (Soria and Ben-  
206 Baruch, 2008). We therefore examined CCR5 expression on various immune and stromal cells in  
207 primary tumors (+dox), regressing tumors (5 days -dox), residual tumors (69 days -dox), and  
208 recurrent tumors by flow cytometry. As expected, Her2 was downregulated following dox  
209 withdrawal in all tumors (Figure 5 – figure supplement 1A). For each cell type, we measured the  
210 median fluorescence intensity (MFI) of CCR5 staining in CCR5+ cells. Interestingly, the level of

211 CCR5 expressed on macrophages increased in residual tumors (Figure 5A and Figure 5 – figure  
212 supplement 2). In contrast, CCR5 expression on CD4+ T cells CD8+ T cells increased in regressing  
213 tumors, but returned to baseline in residual tumors (Figure 5B and C, Figure 5 – figure supplement  
214 2). Similar to macrophages, the expression of CCR5 on fibroblasts was elevated in residual tumors  
215 (Figure 5D, Figure 5 – figure supplement 2). We were also interested in examining CCR5  
216 expression on CD45– tumor cells. We observed a slight increase in CCR5 expression in residual  
217 tumor cells, but otherwise there was no change in CCR5 expression on these cells (Figure 5E). To  
218 directly compare the expression of CCR5 in macrophages and tumor cells, we sorted these two  
219 populations from primary, regressing, residual, and recurrent tumors from MTB;TAN mice and  
220 performed qPCR analysis. CCR5 was expressed at higher levels on macrophages than tumor cells  
221 at each stage, and its expression was especially high on residual tumor macrophages (Figure 5 –  
222 figure supplement 1B). Overall, these results identify several cell types – notably macrophages  
223 and fibroblasts – that express high levels of CCR5 and so are poised to respond to CCL5 in residual  
224 tumors.

225 To determine whether these cell types are recruited by CCL5 in residual tumors, we  
226 generated primary and residual tumors overexpressing CCL5 and analyzed the abundance of  
227 macrophages and fibroblasts by flow cytometry. Fibroblast levels were not significantly different  
228 between control and CCL5-expressing tumors (Figure 5F, Figure 5 – figure supplement 1C). In  
229 contrast, CCL5-expressing tumors exhibited a modest but consistent increase in macrophage  
230 infiltration (Figure 5G, Figure 5 – figure supplement 1D). Taken together, these results suggest  
231 that CCL5 expression in residual tumors can recruit CCR5-positive macrophages, and suggest that  
232 CCL5 may subsequently signal through CCR5 on these cells to modulate macrophage function.

233 **Macrophages express and secrete collagen and collagen deposition factors**

234 We next considered the possibility that CCL5 recruitment of macrophages to residual  
235 tumors may promote recurrence through macrophage-tumor cell crosstalk. To address this, we  
236 sorted CD45<sup>+</sup>/CD11b<sup>+</sup>/F4/80<sup>+</sup> macrophages from primary, residual and recurrent tumors from  
237 the autochthonous MTB;TAN model by fluorescence activated cell sorting (FACS), and then  
238 isolated RNA from the sorted cell populations for RNAseq. Residual tumor-associated  
239 macrophages did not yield sufficient RNA for RNAseq, but we were able to sequence RNA from  
240 primary, regressing, and recurrent tumor-associated macrophages (TAMs). Examination of  
241 differentially expressed genes between primary and recurrent TAMs suggested that FACS-sorted  
242 TAMs may have been partially contaminated with tumor cells. For instance, we detected Her2  
243 expression at high levels in primary TAMs and low levels in recurrent TAMs. Therefore, we used  
244 a gene expression dataset of primary and recurrent tumor cells cultured in vitro to filter the TAM  
245 expression list (Figure 6 – source data 1). After filtering, we were left with approximately 200  
246 genes that were differentially expressed between primary and recurrent tumor macrophages  
247 (Figure 6A, Figure 6 – source data 2). Interestingly, genes encoding fibrillar collagen and collagen  
248 deposition proteins were more highly expressed in the recurrent TAMs than the primary TAMs or  
249 regressing tumor TAMs (Figure 6B). These genes include Collagen alpha-1(V) chain (COL5A1),  
250 Collagen type XXIV alpha 1 (COL24A1), Procollagen C-endopeptidase enhancer 1 (PCOLCE),  
251 and Asporin (ASPN). COL5A1 and COL24A1 encode fibrillar collagens, PCOLCE encodes a  
252 glycoprotein that binds and drives the cleavage of type 1 fibrillar procollagen, and ASPN encodes  
253 a protein that binds to fibrillar collagens to regulate mineralization. We next sought to validate  
254 these findings by performing qPCR analysis on primary, regressing, residual, and recurrent TAMs.  
255 This analysis showed that the expression of these genes progressively increased during tumor  
256 regression, residual disease, and recurrence (Figure 6C). Additionally, qPCR on RNA isolated

257 from bulk tumors showed higher expression of COL5A1 and COL24A1 in recurrent tumors, while  
258 a subset of recurrent tumors had high expression of ASPN and PCOLCE (Figure 6D). Consistent  
259 with this, Masson's trichrome staining showed increased collagen deposition in residual and  
260 recurrent tumors (Figure 6E, middle and bottom). In order to see if similar gene expression patterns  
261 are observed in residual disease in breast cancer patients, we examined gene expression data from  
262 residual tumors after neoadjuvant targeted therapy. Indeed, expression of these four collagen genes  
263 increased in residual tumors following therapy (Figure 6 – figure supplement 1A). Finally, we  
264 asked whether CCL5 regulates collagen deposition by comparing collagen levels in control and  
265 CCL5-expressing recurrent tumors. While control recurrent tumors had uniform levels of collagen  
266 deposition (Figure 6F and Figure 6 – figure supplement 1B-C), a subset of CCL5-expressing  
267 tumors had very high levels of collagen deposition (Figure 6F and Figure 6 – figure supplement  
268 1B-C). Taken together, these results suggest that CCL5 promotes macrophage infiltration and  
269 collagen deposition. Given the importance of collagen for regulating tumor cell function, this may  
270 be one mechanism by which CCL5 expression accelerates recurrence. This is reminiscent of  
271 findings in colorectal cancer, where collagen deposition can be mediated in part through CCR2+  
272 macrophages, and depletion of these macrophages inhibits tumor growth (Afik et al., 2016).

273

## 274 **DISCUSSION**

275 The long-term survival of residual tumor cells following therapy is a major obstacle to  
276 obtaining cures in breast cancer. Understanding the pathways that promote residual cell survival –  
277 and that induce the reactivation of these cells to generate recurrent tumors – is critical for designing  
278 therapies to prevent breast cancer relapse. There has been extensive focus on tumor cell-intrinsic  
279 pathways that allow cells to survive therapy (Holohan et al., 2013). However, the role of tumor

280 cell-extrinsic factors, including the tumor microenvironment, in regulating the survival and  
281 recurrence of residual cells has not been extensively explored.

282 Here we used a conditional mouse model to investigate how interactions between tumor  
283 cells and the tumor microenvironment change during tumor regression, residual disease, and  
284 recurrence, and in turn how the microenvironment regulates tumor recurrence. We found that Her2  
285 downregulation led to induction of a pro-inflammatory gene expression program comprising a  
286 number of chemokines and cytokines, including CCL5. This program was mediated by autocrine  
287 TNF $\alpha$  and dependent upon IKK/NF $\kappa$ B signaling. Notably, a recent study identified a similar gene  
288 expression program in EGFR-mutant lung cancer following treatment with EGFR inhibitors (Gong  
289 et al., 2018). Consistent with this pro-inflammatory gene expression program, we observed  
290 differences in immune and stromal cell infiltration during tumor regression. Both adaptive (CD4+  
291 and CD8+ T cells) and innate (macrophages) immune cells were recruited to regressing tumors.  
292 The residual tumor microenvironment is markedly different from that of primary tumors, with high  
293 numbers of macrophages and fibroblasts, abundant collagen deposition, and differential expression  
294 of a suite of cytokines, including CCL5. Functionally, CCL5 overexpression promotes  
295 macrophage recruitment, collagen deposition, and promotes tumor recurrence. These results  
296 identify CCL5 as a critical regulator of crosstalk between residual tumor cells and the residual  
297 tumor microenvironment that promotes tumor recurrence.

298 A number of studies have found that Her2 signaling directly activates the NF $\kappa$ B pathway,  
299 and that this is functionally important for tumor growth (Liu et al., 2009). Consistent with this, we  
300 observed basal levels of p65 phosphorylation in primary tumor cells. Surprisingly, we found that  
301 Her2 inhibition further activates the NF $\kappa$ B pathway, and that this occurs through an autocrine  
302 pathway that is likely mediated by increased TNF $\alpha$  expression. Hyperactivation of the NF $\kappa$ B

303 pathway in turn leads to the production of a number of cytokines and chemokines which may  
304 contribute to the recruitment of immune cells. These findings are consistent with prior work  
305 showing that the NF $\kappa$ B pathway is required for macrophage recruitment in a similar Her2-driven  
306 mouse model (Liu et al., 2010). Our findings add to these previous studies by showing that Her2  
307 inhibition leads to hyperactivation of the NF $\kappa$ B pathway and increased macrophage recruitment.

308 CCL5 has been shown to play an important role in many facets of tumor progression, such  
309 as invasion, metastasis, neoangiogenesis, and immune cell infiltration (Aldinucci and Colombatti,  
310 2014). In glioblastoma, CCL5 upregulation has been correlated with recurrence in post-treatment  
311 tumors (Hudson et al., 2018). In triple-negative breast cancer, CCL5 expression has also been  
312 correlated with residual tumor size and tumor infiltrating lymphocytes after neoadjuvant  
313 chemotherapy (Araujo et al., 2018). However, CCL5 has not previously been implicated in residual  
314 cell survival or recurrence in Her2+ or hormone receptor positive breast cancer. By analyzing gene  
315 expression datasets from breast cancer patients treated with neoadjuvant targeted or chemotherapy  
316 (Creighton et al., 2009; Tempfer, 2011), we show here that CCL5 expression is elevated in residual  
317 tumor cells that survive therapy. A notable observation in our study is that while CCL5 expression  
318 promoted recurrence (Figure 4C), knockout of CCL5 in tumor cells did not delay recurrence  
319 (Figure 4E). This suggests that CCL5 may be at least partially redundant with other chemokines,  
320 such as CCL2 and CXCL1 and 2, in recruiting macrophages to promote recurrence.

321 Mechanistically, we show that CCL5 acts to recruit CCR5+ macrophages to residual  
322 tumors, consistent with its known role as a chemoattractant factor for macrophages (Mantovani et  
323 al. 2017). RNAseq analysis of primary and recurrent TAMs suggested that recurrent TAMs have  
324 high expression of genes encoding fibrillar collagen and proteins required for collagen deposition.  
325 qPCR analysis indicated that residual TAMs shared this gene expression program. Consistent with



326 this, collagen deposition is high in residual and recurrent tumors, and CCL5 expression promotes  
327 collagen deposition. Collagen deposition is traditionally thought to be driven by fibroblasts in the  
328 microenvironment (Thannickal, 2012). However, a recent report showed that macrophages are  
329 responsible for collagen deposition in a mouse model of colorectal cancer (Afik et al., 2016).  
330 Collagen deposition is important for tumor progression and invasiveness (Provenzano et al., 2008).  
331 Collagen bundles can potentiate cell migration and increase tissue stiffness, and enzymes which  
332 crosslink collagens are often upregulated in breast cancer and are correlated with a poor prognosis  
333 (Lu et al., 2012). It is possible that collagen deposition may promote the survival or proliferation  
334 of residual tumor cells, and that this mediates the effect of CCL5 on tumor recurrence.

335 The findings reported here suggest that efforts to block CCL5-driven macrophage  
336 infiltration and subsequent collagen deposition may have therapeutic benefit. Possible therapies  
337 include the use of Maraviroc, a CCR5 antagonist (Velasco-Velazquez et al., 2012), and agents that  
338 block macrophage infiltration or function, such as the CSF-1R inhibitor PLX3397 (DeNardo et al.,  
339 2011; Strachan et al., 2014; Zhu et al., 2014). It is also possible that, because CCL5 is sufficient  
340 but not necessary for tumor recurrence, it would be preferable to block the induction of the pro-  
341 inflammatory program that is induced following Her2 downregulation using agents targeting  
342 TNF $\alpha$  or the NF $\kappa$ B pathway.

343 It is important to note that while our studies focus on the function of CCL5 in recruiting  
344 CCR5+ macrophages, breast cancer cells themselves can also express CCR5. Indeed, previous  
345 studies have found that CCR5 acts in tumor cells to promote stem cell expansion and metastasis  
346 in breast cancer (Jiao et al., 2018; Velasco-Velazquez et al., 2012). Although in the current study  
347 we find that in residual tumors CCR5 is expressed at higher levels in macrophages than on tumor  
348 cells, it is possible that tumor cell-expressed CCR5 may mediate at least some of the effects of

349 CCL5 on tumor recurrence. Future work with mice lacking CCR5 on specific cell types will clarify  
 350 the relative important of CCR5 on macrophages and tumor cells.

351 The survival and recurrence of residual tumor cells is a critical clinical problem in breast  
 352 cancer. The results identified here show that interactions between residual tumor cells and their  
 353 microenvironment are critical for recurrent tumor formation. Targeting tumor cell-  
 354 microenvironment interactions may hold promise for preventing recurrent breast cancer.

355

## 356 MATERIALS AND METHODS

### 357 Key resources table

Reagent type (species) or resource	Designation	Source or reference	Identifiers	Additional Information
Recombinant DNA reagent	pLenti CMV GFP Neo	Addgene	Plasmid # 17447 RRID:Addgene_17447	Campeau et al PLoS One. 2009 Aug 6;4(8):e6529
Recombinant DNA reagent	lentiCas9-Blast	Addgene	Plasmid # 52962 RRID:Addgene_52962	Sanjana et al Nat Methods. 2014 Aug;11(8):783-4
Recombinant DNA reagent	lentiGuide-Puro	Addgene	Plasmid # 52963 RRID:Addgene_52963	Sanjana et al Nat Methods. 2014 Aug;11(8):783-4
Recombinant DNA reagent	psPAX2	Addgene	Plasmid # 12260 RRID:Addgene_12260	Trono Lab Packing and Envelope Plasmids
Recombinant DNA reagent	pMD2.G	Addgene	Plasmid# 12259 RRID:Addgene_12259	Trono Lab Packing and Envelope Plasmids

Cell line ( <i>M. musculus</i> )	NIH-3T3	American Type Culture Collection	Cat# CRL-1658 RRID:CVCL_0594	
Cell line ( <i>M. musculus</i> )	54074	This paper		Derived from MTB;TAN model
Cell line ( <i>M. musculus</i> )	99142	This paper		Derived from MTB;TAN model
Cell line ( <i>H. Sapiens</i> )	293T Ampho	American Type Culture Collection	Cat# CRL-3213 RRID:CVCL_H716	
Cell line ( <i>H. Sapiens</i> )	293T Eco	American Type Culture Collection	Cat# CRL-3214 RRID:CVCL_H717	
Antibody	Rabbit monoclonal anti-NFκB p65	Cell Signaling	D14E12 RRID:AB_10859369	1:1000 (WB)
Antibody	Rabbit monoclonal anti-p-NFκB p65	Cell Signaling	93H1 RRID:AB_10827881	1:1000 (WB)
Antibody	Mouse monoclonal anti-Tubulin	Santa Cruz	TU-02 RRID:AB_628408	1:1000 (WB)
Antibody	Goat anti-rabbit HRP	Cell Signaling	Cat# 7074 RRID:AB_2099233	1:5000 (WB)
Antibody	Goat anti-mouse HRP	Cell Signaling	Cat# 7076 RRID:AB_330924	1:5000 (WB)
Antibody	Goat anti-rabbit Alexa Flour 680	Life Technologies	Cat# A21076 RRID:AB_141386	1:5000 (WB)

Antibody	IRDYE 800CW Goat anti-mouse	LI-COR	Cat# 926-32210 RRID:AB_621842	1:5000 (WB)
Antibody	Rat monoclonal anti-CD45R/B220, APC conjugated	Invitrogen/eBioscience (Carlsbad, CA)	RA3-6B2 RRID:AB_469395	1:50 (FC)
Antibody	Hamster monoclonal anti-CD49b, AF488 conjugated	BioLegend	HM $\alpha$ 2 RRID:AB_492851	1:200 (FC)
Antibody	Hamster monoclonal anti-Fc $\epsilon$ RI $\alpha$ , PE conjugated	BioLegend	1-Mar RRID:AB_1626104	1:50 (FC)
Antibody	Rat monoclonal anti-Siglec-F/CD170, PE conjugated	BD	E50-2440 RRID:AB_10896143	1:200 (FC)
Antibody	Rat monoclonal anti-PDGFR $\alpha$ /CD140a, PE conjugated	Invitrogen/eBioscience	APA5 RRID:AB_657615	1:100 (FC)
Antibody	Rat monoclonal anti-CD45, PECy5 conjugated	BD	30-F11 RRID:AB_394612	1:200 (FC)
Antibody	Mouse monoclonal anti-CD45, APC conjugated	BD	30-F11 RRID:AB_1645215	1:200 (FC)
Antibody	Rat anti-CD45, V50 conjugated	BD	30-F11 RRID:AB_1645275	1:200 (FC)

Antibody	Rat monoclonal anti-F4/80, AF647 conjugated	BD	T45-2342 RRID:AB_2744474	1:50 (FC)
Antibody	Rat monoclonal anti-CD11b, PE conjugated	BD	M1/70 RRID:AB_394775	1:50 (FC)
Antibody	Rat monoclonal anti-CD11b, PECy7 conjugated	BD	M1/70 RRID:AB_2033994	1:100 (FC)
Antibody	Rat monoclonal anti-Ly6G, APC conjugated	BD	1A8 RRID:AB_1727560	1:200 (FC)
Antibody	Hamster monoclonal anti-CD3e, PE conjugated	BD	145-2C11 RRID:AB_394460	1:100 (FC)
Antibody	Rat monoclonal anti-CD4, APCC7y conjugated	BD	GK1.5 RRID:AB_394331	1:100 (FC)
Antibody	Rat monoclonal anti-CD8a, APC conjugated	BD	53-6.7 RRID:AB_398527	1:200 (FC)
Antibody	Rat monoclonal anti-CD16/CD32 Fc Blocker	BD	2.4G2 RRID:AB_394659	1:50 (FC)
Antibody	Rat monoclonal anti-CCR5/CD195, BV421 conjugated	BD	C34-3448 RRID:AB_2741677	1:100 (FC)

Antibody	Mouse monoclonal anti-Cytokertin 8	Troma 1, Brulet, P., Kemler, R. Institut Pasteur, Paris, France	Troma 1 RRID:AB_531826	1:50 (IHC)
Antibody	Rat monoclonal anti-CD45	BD Biosciences	30-F11 RRID:AB_394606	1:200 (IHC)
Antibody	Rabbit monoclonal anti-CD3	Thermo	SP7 RRID:AB_1956722	1:100 (IHC)
Antibody	Rat monoclonal anti-F4/80	Bio-Rad	Cl:A3-1 RRID:AB_1102558	1:1000 (IHC)
Peptide, recombinant protein	TNF $\alpha$ , mouse	BioLegend	Cat# 575202	10 ng/mL
Commercial assay or kit	Trichrome stain	Abcam	ab150686	
Commercial assay or kit	Vectastain ABC Kit (Rabbit IgG)	Vector Labs	Cat# PK-6101	
Commercial assay or kit	Vectastain ABC Kit (Rat IgG)	Vector Labs	Cat# PK-4004	
Commercial assay or kit	RNeasy Mini Kit	Qiagen	Qiagen:74106	
Commercial assay or kit	QIAshredder	Qiagen	Qiagen:79656	
Commercial assay or kit	Quantibody Mouse Cytokine Array Q1	RayBiotech	Cat# QAM-CYT-1-1	
Commercial	Quantibody Mouse	RayBiotech	Cat# QAM-CYT-4	

assay or kit	Cytokine Array Q4			
Chemical compound, drug	IKK16	Selleckchem	Cat# S2882	100nM
Chemical compound, drug	Lipofectamine 2000	Life Technologies	Cat# 11668019	60 $\mu$ L per reaction
Chemical compound, drug	Polybrene	Sigma	Cat# 107689	6 $\mu$ g/mL
Chemical compound, drug	2x Cell Lysis Buffer	RayBiotech	Cat# AA-LYS	
Chemical compound, drug	Luminata Classico/Crescendo Western HRP Substrate	Millipore	Cat#WBLUC0500 Cat#WBLUR0500	
Chemical compound, drug	Doxycycline	RPI	Cat# D43020-100.0	2 mg/kg <i>in vivo</i> and 2 $\mu$ g/mL <i>in vitro</i>
Sequence-based reagent	RT-PCR primers	This paper	CCL5 cDNA into pK1 plasmid	Forward: TAACCTCGAGATGAAGATC TCTGCAGCTG, Reverse: TAACGCGGCCCGCCAGGGTC AGAATCAAGAAACC
Sequence-based reagent	RT-PCR primers	This paper	CCL5 cDNA into pLenti CMV plasmid	Forward: TAACTCTAGAATGAAGATC TCTGCAGCTG, Reverse: TAACGTTCGACCAGGGTCAG AATCAAGAAACC

Sequencing-based reagent	gRNAs	This paper	Targeting CCL5	CCL5_1 (TG TAGAAATACTCCTTGACG), CCL5_2 (TACTCCTTGACGTGGGCACG), CCL5_3 (TGCAGAGGGCGGCTGCAGTG)
Sequencing-based reagent	CCL5	Thermo	Mm0130242 7_m1	
Sequencing-based reagent	CXCL1	Thermo	Mm0420746 0_m1	
Sequencing-based reagent	CXCL2	Thermo	Mm0043645 0_m1	
Sequencing-based reagent	CXCL5	Thermo	Mm0043645 1_g1	
Sequencing-based reagent	CCL2	Thermo	Mm0044124 2_m1	
Sequencing-based reagent	Actin	Thermo	Mm0261958 0_g1	
Sequencing-based reagent	ASPN	Thermo	Mm0044594 5_m1	
Sequencing-based reagent	PCOLCE	Thermo	Mm0047660 8_m1	
Sequencing-based reagent	COL5A1	Thermo	Mm0048929 9_m1	
Sequencing-based reagent	COL24A1	Thermo	Mm0132374 4_m1	



based reagent				
Software, algorithm	GraphPad Prism	GraphPad Prism ( <a href="https://graphpad.com">https://graphpad.com</a> )	RRID:SCR_002798	Version 8
Software, algorithm	JMP Pro	SAS Institute Inc., Cary, NC		
Software, algorithm	FlowJo	TreeStar	RRID:SCR_008520	
Software, algorithm	Fiji	Fiji ( <a href="http://fiji.nih.gov/">http://fiji.nih.gov/</a> )	RRID:SCR_002285	Schindelin, J.; Arganda-Carreras, I. & Frise, E. et al. (2012) Nature methods 9(7):676-682

358 **WB = Western blot, FC = flow cytometry, IHC = immunohistochemistry**

### 359 **Orthotopic recurrence assays**

360 Orthotopic tumor recurrence assays were performed as described (Alvarez et al. 2013).  
 361 Briefly, cohorts of 6-week old recipient mice (nu/nu or TAN) on doxycycline were injected  
 362 bilaterally in the #4 inguinal mammary fat pad with  $1 \times 10^6$  primary tumor cells (expressing either  
 363 a control sgRNA, a sgRNA targeting CCL5, CCL5 cDNA, or GFP cDNA). Once tumors reached  
 364 5 mm (2-3 weeks), doxycycline was removed to initiate oncogene down-regulation and tumor  
 365 regression. Mice were palpated biweekly to monitor tumor recurrence, and sacrificed when  
 366 recurrent tumors reached 10 mm. Differences in recurrence-free survival between control and  
 367 experimental cohorts were compared using Kaplan-Meier survival curves (L et al., 1958) and  
 368 evaluated by the p-value from a log-rank test and the hazard ratio from the Cox proportional hazard  
 369 regression, as described previously (Alvarez et al., 2013).

370 Power calculations were used to determine cohort size for each in vivo experiment.  
 371 Briefly, in order to detect a 2.5-fold difference in recurrence-free survival between control and

372 experimental groups, given a median recurrence-free survival of 60 days for the control group and  
373 a 300-day follow-up, we estimated we would need to enroll 22 tumors per group (80% power,  
374  $p < 0.05$ ). We enrolled extra mice in each cohort to account for tumor take rates and unexpected  
375 mortality. Final cohort sizes were: GFP tumors, 17 mice (34 tumors); CCL5 tumors, 18 mice (36  
376 tumors); sgControl tumors, 20 mice (40 tumors); sgCCL5 tumors, 20 mice (40 tumors).

### 377 **Tissue culture and reagents**

378 Cell lines derived from primary MTB;TAN tumors were grown as previously described in  
379 media containing 2  $\mu\text{g/ml}$  dox (Alvarez et al., 2013). For conditioned media experiments, primary  
380 tumor cell lines were plated on 10-cm plates. 24 hours later, media was changed to media without  
381 dox, and conditioned media was collected one or two days later. Media was centrifuged to remove  
382 cells, supplemented with 2  $\mu\text{g/ml}$  dox, and applied to naïve primary tumor cells. Cells treated with  
383 conditioned media were harvested one or two days later for qPCR or Western blot analysis. For  
384 dox withdrawal experiments, primary tumor cell lines were plated 10-cm plates. 24 hours later,  
385 media was changed to media without dox and cells were collected one or two days later for qPCR  
386 or Western blot analysis. IKK16 (Selleckchem, Houston, TX) was used at 100 nM, TNF $\alpha$   
387 (BioLegend, San Diego, CA) was used at 10 ng/ml.

388 Primary cells derived from MTB;TAN tumors (54074 and 99142 cells) were generated by  
389 our lab, are used at early passages, and as a result have not been authenticated. NIH3T3 cells were  
390 tested by the Duke Cell Culture Facility for mycoplasma contamination and tested negative. The  
391 facility was not able to perform STR authentication on these mouse cells.

392

### 393 **Flow cytometry**

394 Tumors were harvested and digested as previously described (Mabe et al., 2018). Cells  
 395 were aliquoted at  $1 \times 10^6$  cells per 5 mL falcon tube. CD16/CD32 Fc Block antibody was added for  
 396 10 min at 4°C (2  $\mu$ L/ $1 \times 10^6$  cells). Tumors were then stained with antibody cocktails listed below  
 397 for 30 min at 4°C, and then washed 3 times with FACs buffer (BD Biosciences, Billerica, MA).

Cell Type	Antibody	Fluorophore	Clone	Vendor	Dilution
B Cell	CD45R/B220	APC	RA3-6B2	Invitrogen/eBioscience (Carlsbad, CA)	1:50
Basophil	CD49b	AF488	HM $\alpha$ 2	BioLegend	1:200
Basophil	Fc $\epsilon$ RI $\alpha$	PE	MAR-1	BioLegend	1:50
Eosinophil	Siglec-F/CD170	PE	E50-2440	BD	1:200
Fibroblast	PDGFR $\alpha$ /CD140a	PE	APA5	Invitrogen/eBioscience	1:100
Leukocyte	CD45	PECy5	30-F11	BD	1:200
Leukocyte	CD45	APC	30-F11	BD	1:200
Leukocyte	CD45	V450	30-F11	BD	1:200
Macrophage	F4/80	AF647	T45-2342	BD	1:50
Monocyte/Granulocyte	CD11b	PE	M1/70	BD	1:50
Monocyte/Granulocyte	CD11b	PECy7	M1/70	BD	1:100
Neutrophil	Ly6G	APC	1A8	BD	1:200
T Cell	CD3e	PE	145-2C11	BD	1:100
T Cell	CD4	APCCy7	GK1.5	BD	1:100
T Cell	CD8a	APC	53-6.7	BD	1:200
-	Fc Blocker	-	2.4G2	BD	1:50
-	CCR5/CD195	BV421	C34-3448	BD	1:100

398  
 399 Cells were analyzed using a FACSCanto analyzer (BD Biosciences) and data were analyzed using  
 400 FlowJo software (TreeStar, Ashland, OR). Gating of the CCR5-high population was determined  
 401 by using a fluorescence minus one (FMO; cells stained with antibodies for cell type markers,  
 402 lacking the CCR5 antibody) histogram in the fluorescence channel for the CCR5 antibody as a

403 negative control. The FMO negative control histogram was plotted with a positive control of the  
404 single stain (cells stained only with CCR5 antibody) from the same tumor. Percent of CCR5+ cells  
405 were gated according to the positive control.

#### 406 **qPCR**

407 RNA was isolated from tumors and cells using RNeasy columns (Qiagen, Hilden,  
408 Germany). 1 µg of RNA was reversed transcribed using cDNA synthesis reagents (Promega,  
409 Madison, WI). qPCR was performed using 6-carboxyfluorescein labeled TaqMan probes  
410 (Thermo, Waltham, MA): CCL5 (Mm01302427\_m1), CXCL1 (Mm04207460\_m1), CXCL2  
411 (Mm00436450\_m1), CXCL5 (Mm00436451\_g1), CCL2 (Mm00441242\_m1), Actin  
412 (Mm02619580\_g1), ASPN (Mm00445945\_m1), PCOLCE (Mm00476608\_m1), COL5A1  
413 (Mm00489299\_m1), COL24A1 (Mm01323744\_m1), and read on a Bio-Rad (Hercules, CA)  
414 CFX qPCR machine.

#### 415 **Western blotting and cytokine arrays**

416 Western blotting was performed as described (Alvarez et al. 2013) using the following  
417 antibodies: NFκB p65 (D14E12, Cell Signaling, Danvers, MA), p-NFκB p65 (93H1, Cell  
418 Signaling), and tubulin (TU-02, Santa Cruz, Dallas, TX), all at a 1:1000 dilution. Secondary  
419 antibodies conjugated to Alexa Flour 680 (Life Technologies, Carlsbad, CA) or 800 (LI-COR  
420 Biosciences, Lincoln, NE) were detected with the Odyssey detection system (LI-COR  
421 Biosciences). For p-p65 detection, secondary antibodies conjugated to HRP were used and blots  
422 were developed using Classico or Crescendo reagent (Millipore, Burlington, MA) and exposed to  
423 film (VWR, Radnor, PA). Secondary antibodies were used at a 1:5000 dilution.

424 For cytokine array analysis, tumor lysates were made in 2X lysis buffer (RayBiotech,  
425 Norcross, GA) and diluted to 50 µg per 100 µL in diluent provided. Tumor lysates and standards

426 were run on both Quantibody Mouse Cytokine Array Q1 and Q4 (RayBiotech). Slides were  
427 scanned and quantified by RayBiotech.

#### 428 **Plasmids and CRISPR/Cas9**

429 pLenti CMV GFP Puro was purchased from Addgene (Watertown, MA).

430 A CCL5 cDNA encoding the full-length mouse protein was amplified by RT-PCR from  
431 recurrent MTB;TAN tumor cells and cloned into the retroviral expression vector pK1 using the  
432 following primers: Forward: TAACCTCGAGATGAAGATCTCTGCAGCTG, Reverse:  
433 TAACGCGGCCGCCAGGGTCAGAATCAAGAAACC.

434 A CCL5 cDNA encoding the full-length mouse protein was amplified by RT-PCR from  
435 recurrent MTB;TAN tumor cells and cloned into the lentiviral expression vector pLenti CMV  
436 using the following primers: Forward: TAACTCTAGAATGAAGATCTCTGCAGCTG, Reverse:  
437 TAACGTCGACCAGGGTCAGAATCAAGAAACC.

438 CCL5 CRISPR sgRNAs: CCL5\_1 (TG TAGAAATACTCCTTGACG), CCL5\_2  
439 (TACTCCTTGACGTGGGCACG), CCL5\_3 (TGCAGAGGGCGGCTGCAGTG). A small guide  
440 against AAVS was used as control. sgRNAs were cloned into Lentiguide puro (Sanjana et al.  
441 2014). Cas9 infection was with lentiguide Cas9 blast (Sanjana et al. 2014).

442 Retrovirus was produced by transfecting the packaging lines 293T Ampho and 293T Eco  
443 with the retroviral construct pK1 empty or CCL5 using Lipofectamine 2000. Retroviral  
444 supernatant was collected 48 hours post-transfection, filtered, and used to transduce cells in the  
445 presence of 6 µg/mL polybrene (Sigma, St. Louis, MO).

446 Lentivirus was produced by transfecting 293T cells with the packaging plasmids psPAX2  
447 and pMD2.G and lentiviral construct pLenti CMV GFP or CCL5 using Lipofectamine 2000.

448 Lentiviral supernatant was collected 48 hours post-transfection, filtered, and used to transduce  
449 cells in the presence of 6 µg/mL polybrene (Sigma).

#### 450 **RNA sequencing**

451 RNA was isolated from tumors or tumor cells using RNeasy columns (Qiagen). For TAM  
452 sequencing, macrophages were isolated by FACS using the antibody panel described above, and  
453 RNA was isolated using RNeasy columns (Qiagen). RNA was sequenced using the Illumina HiSeq  
454 4000 libraries and sequencing platform with 50 base pair single end reads by the Duke GCB  
455 Sequencing and Genomic Technologies Shared Resource (Durham, NC). Sequencing data have  
456 been deposited in SRA as PRJNA506006 for cell line data and PRJNA505845 for macrophage  
457 data.

#### 458 **Human breast cancer microarray data**

459 Publicly available microarray data from human primary and residual breast cancer datasets  
460 GSE10281 and GSE21974 and their corresponding clinical annotation were downloaded,  
461 converted to log<sub>2</sub> scale, and median centered. Heatmaps were created using R (Team, 2013).

#### 462 **Immunohistochemistry and staining**

463 Tumor sections were fixed in 10% normal formalin for 16 hours, then washed twice with  
464 PBS and transferred to 70% ethanol for storage. Stored tumor sections were paraffin imbedded  
465 and cut on the microtome in 5 µm sections. Sections were stained using a regressive H&E protocol,  
466 immunohistochemistry, or Masson's Trichrome.

467 The regressive H&E protocol is as follows: dewax and rehydrate slides. Incubate slides in  
468 Harris Modified Hematoxylin with Acetic Acid (Fisher, Hampton, NH) for 5 min. Incubate in  
469 Eosin (Sigma) for 1:30 min. Then dehydrate slides and mount slides with permount and coverslip.  
470 Let dry overnight.

471 For cytokeratin 8 staining (Troma 1, Brulet, P., Kemler, R. Institut Pasteur, Paris, France)  
472 immunohistochemistry slides were dewaxed and rehydrated as above. Slides were boiled in  
473 antigen retrieval buffer (1X in ddH<sub>2</sub>O) for 5 minutes and allowed to cool. Slides were washed in  
474 PBS and then incubated in 0.3% H<sub>2</sub>O<sub>2</sub>. Slides were washed, blocked and stained according to the  
475 protocol from the rabbit secondary Vectastain ABC kit (Vector Labs, Burlingame, CA). Primary  
476 antibody was used at a dilution of 1:50. CD45 (30-F11, BD Biosciences, 1:200), CD3 (SP7,  
477 Thermo, 1:100), and F4/80 (Cl:A3-1, Bio-Rad, 1:1000) staining were performed by the Duke  
478 Pathology core (Durham, NC).

479 Trichrome stain was performed using a staining kit from Abcam (Cambridge, UK)  
480 (ab150686).

#### 481 **Quantifying IHC and Masson's Trichrome in Fiji**

482 To quantify the amount of positive staining for CD3, CD45, and F4/80 and for Masson's  
483 Trichrome, we used Fiji (Schindelin et al., 2012). The 'Color Deconvolution' function was used  
484 to separate the colors into positive staining and hematoxylin for normalization. We then  
485 converted each image to 8-bit and applied a threshold of positive staining to each image and used  
486 this same threshold across all images. We then measured the pixel area of the positive staining  
487 and normalized this to the hematoxylin staining for each image. For the primary tumors and 5-  
488 day -dox tumors, the whole image was used for quantification. For residual tumors we manually  
489 selected regions-of-interest to exclude adipose tissue from the quantification.

#### 490 **Statistical reporting**

491 For GSEA, the normalized enrichment score (NES) is reported. The normalized enrichment  
492 score accounts for differences in gene set size and in correlations between gene sets. The NES is  
493 based on all dataset permutations, to correct for multiple hypothesis testing. The nominal p value

494 is also reported, and is the statistical significance of the enrichment score, without adjustment for  
495 gene set size or multiple hypothesis testing. A reported p value of zero (0.0) indicates an actual p-  
496 value of less than 1/number-of-permutations. (Subramanian et al., 2005)

497 Two-tailed unpaired t-tests were used to analyze significance between primary tumor  
498 samples and all other time points for qPCR, cytokine array, and flow cytometry analysis. For the  
499 cytokine array, appropriate same size was calculated using JMP Pro (SAS Institute Inc., Cary,  
500 NC). A standard deviation of 20% was assumed, with a power of 0.8, fold change of 2, and p-  
501 value (alpha) of 0.05. This power calculation indicated that a sample size of 8 (4 tumors per cohort)  
502 was required. The same parameters were used for sample size calculation for flow cytometry  
503 analysis of control and CCL5-expressing tumors. For recurrence free survival (RFS), statistical  
504 analysis methods are listed in orthotopic recurrence assays.

505 Outliers were never excluded except for in flow cytometry experiments. Tumors that were  
506 >90% CD45+ were excluded from analysis to avoid analyzing tumors with potential contamination  
507 from the inguinal lymph node. For all other experiments where no power analysis was used, sample  
508 size was chosen based upon previous experience (Alvarez et al., 2013).

#### 509 **Study approval**

510 Animal care and all animal experiments were performed with the approval of and in  
511 accordance with Duke University IACUC guidelines. Mice were housed under barrier conditions.

#### 512 **Funding**

513 This work was funded by the National Cancer Institute (R01 CA208042 to JVA and F31  
514 CA220957 to AW) and by startup funds from the Duke Cancer Institute, the Duke University  
515 School of Medicine and the Whitehead Foundation (to JVA).

#### 516 **Acknowledgements**



517           We thank Cui Rong (Duke-NUS, Singapore) for providing technical assistance, as well as  
518 members of the Alvarez lab for providing assistance and helpful discussions. We thank Dr. Mike  
519 Cook (Duke University) and Dr. Brent Hanks (Duke University) for assistance with flow  
520 cytometry. We thank Dr. So Young Kim (Duke University) for reagents for the CRISPR-Cas9 cell  
521 lines. We also thank Dr. Donald McDonnell, Dr. Binita Das, and Dr. Ching-Yi Chang (Duke  
522 University) for providing assistance and reagents for flow cytometry.

523  
524  
525

526 **REFERENCES**

527

528 Afik, R., Zigmund, E., Vugman, M., Klepfish, M., Shimshoni, E., Pasmanik-Chor, M., Shenoy,  
529 A., Bassat, E., Halpern, Z., Geiger, T., *et al.* (2016). Tumor macrophages are pivotal constructors  
530 of tumor collagenous matrix. *The Journal of experimental medicine* 213, 2315-2331.

531 Aldinucci, D., and Colombatti, A. (2014). The inflammatory chemokine CCL5 and cancer  
532 progression. *Mediators of inflammation* 2014, 292376.

533 Alexander-Savino, C.V., Hayden, M.S., Richardson, C., Zhao, J., and Poligone, B. (2016).  
534 Doxycycline is an NF- $\kappa$ B inhibitor that induces apoptotic cell death in malignant T-cells.  
535 *Oncotarget* 7, 75954-75967.

536 Alvarez, J.V., Pan, T.-c., Ruth, J., Feng, Y., Zhou, A., Pant, D., Grimley, J.S., Wandless, T.J.,  
537 DeMichele, A., and Chodosh, L.A. (2013). Par-4 Downregulation Promotes Breast Cancer  
538 Recurrence by Preventing Multinucleation following Targeted Therapy. *Cancer cell* 24, 30-44.

539 Araujo, J.M., Gomez, A.C., Aguilar, A., Salgado, R., Balko, J.M., Bravo, L., Doimi, F., Bretel,  
540 D., Morante, Z., Flores, C., *et al.* (2018). Effect of CCL5 expression in the recruitment of  
541 immune cells in triple negative breast cancer. In *Scientific reports*, pp. 4899.

542 Binnewies, M., Roberts, E.W., Kersten, K., Chan, V., Fearon, D.F., Merad, M., Coussens, L.M.,  
543 Gabrilovich, D.I., Ostrand-Rosenberg, S., Hedrick, C.C., *et al.* (2018). Understanding the tumor  
544 immune microenvironment (TIME) for effective therapy. *Nature medicine*, 1-10.

545 Creighton, C.J., Li, X., Landis, M., Dixon, J.M., Neumeister, V.M., Sjolund, A., Rimm, D.L.,  
546 Wong, H., Rodriguez, A., Herschkowitz, J.I., *et al.* (2009). Residual breast cancers after  
547 conventional therapy display mesenchymal as well as tumor-initiating features. *Proceedings of*  
548 *the National Academy of Sciences of the United States of America* 106, 13820-13825.

549 Damrauer, J.S., Phelps, S.N., Amuchastegui, K., Lupo, R., Mabe, N.W., Walens, A., Kroger,  
550 B.R., and Alvarez, J.V. (2018). Foxo-dependent Par-4 Upregulation Prevents Long-term  
551 Survival of Residual Cells Following PI3K–Akt Inhibition. *Molecular Cancer Research*.

552 Dembic, Z. (2015). *Cytokines of the Immune System: Chemokines* (Academic Press).

553 DeNardo, D.G., Brennan, D.J., Rexhepaj, E., Ruffell, B., Shiao, S.L., Madden, S.F., Gallagher,  
554 W.M., Wadhvani, N., Keil, S.D., Junaid, S.A., *et al.* (2011). Leukocyte Complexity Predicts  
555 Breast Cancer Survival and Functionally Regulates Response to Chemotherapy. *Cancer*  
556 *discovery* 1, 54-67.

557 Flores-Borja, F., Irshad, S., Gordon, P., Wong, F., Sheriff, I., Tutt, A., and Ng, T. (2016).  
558 Crosstalk between Innate Lymphoid Cells and Other Immune Cells in the Tumor  
559 Microenvironment. *Journal of Immunology Research* 2016, 1-14.

560 Gong, K., Guo, G., Gerber, D.E., Gao, B., Peyton, M., Huang, C., Minna, J.D., Hatanpaa, K.J.,  
561 Kernstine, K., Cai, L., *et al.* (2018). TNF-driven adaptive response mediates resistance to EGFR  
562 inhibition in lung cancer. *The Journal of clinical investigation* 128, 2500-2518.

- 563 Hata, A.N., Niederst, M.J., Archibald, H.L., Gomez-Caraballo, M., Siddiqui, F.M., Mulvey,  
564 H.E., Maruvka, Y.E., Ji, F., Bhang, H.-e.C., Krishnamurthy Radhakrishna, V., *et al.* (2016).  
565 Tumor cells can follow distinct evolutionary paths to become resistant to epidermal growth  
566 factor receptor inhibition. *Nature medicine* 22, 262-269.
- 567 Holohan, C., Van Schaeybroeck, S., Longley, D.B., and Johnston, P.G. (2013). Cancer drug  
568 resistance: an evolving paradigm. *Nature Reviews Cancer* 13, 714.
- 569 Hölzel, D., Eckel, R., Emeny, R.T., and Engel, J. (2010). Distant metastases do not metastasize.  
570 *Cancer and Metastasis Reviews* 29, 737-750.
- 571 Hudson, A.L., Parker, N.R., Khong, P., Parkinson, J.F., Dwight, T., Ikin, R.J., Zhu, Y., Chen, J.,  
572 Wheeler, H.R., and Howell, V.M. (2018). Glioblastoma Recurrence Correlates With Increased  
573 APE1 and Polarization Toward an Immuno-Suppressive Microenvironment. *Frontiers in*  
574 *oncology* 8, 314-314.
- 575 Jiao, X., Velasco-Velazquez, M.A., Wang, M., Li, Z., Rui, H., Peck, A.R., Korkola, J.E., Chen,  
576 X., Xu, S., DuHadaway, J.B., *et al.* (2018). CCR5 Governs DNA Damage Repair and Breast  
577 Cancer Stem Cell Expansion. *Cancer research* 78, 1657-1671.
- 578 Klein, C.A. (2009). Parallel progression of primary tumours and metastases. *Nature Reviews*  
579 *Cancer* 9, 302.
- 580 L, E., Kaplan, and Meier, P. (1958). Nonparametric Estimation From Incomplete Observations.  
581 *Journal of the American Statistical Association* 53, 457-481.
- 582 Lacy, P. (2017). Eosinophil Cytokines in Allergy. In (Academic Press), pp. 173-218.
- 583 Lee, C.-M., Peng, H.-H., Yang, P., Liou, J.-T., Liao, C.-C., and Day, Y.-J. (2017). C-C  
584 Chemokine Ligand-5 is critical for facilitating macrophage infiltration in the early phase of liver  
585 ischemia/reperfusion injury. *Scientific Reports* 7, 3698.
- 586 Lee, R.J., Albanese, C., Fu, M., Amico, M., Lin, B., Watanabe, G., Haines, G.K., Siegel, P.M.,  
587 Hung, M.-C., Yarden, Y., *et al.* (2000). Cyclin D1 Is Required for Transformation by Activated  
588 Neu and Is Induced through an E2F-Dependent Signaling Pathway. *Molecular and cellular*  
589 *biology* 20, 672.
- 590 Liu, M., Ju, X., Willmarth, N.E., Casimiro, M.C., Ojeifo, J., Sakamaki, T., Katiyar, S., Jiao, X.,  
591 Popov, V.M., Yu, Z., *et al.* (2009). Nuclear factor-kappaB enhances ErbB2-induced mammary  
592 tumorigenesis and neoangiogenesis in vivo. *The American journal of pathology* 174, 1910-1920.
- 593 Liu, M., Sakamaki, T., Casimiro, M.C., Willmarth, N.E., Quong, A.A., Ju, X., Ojeifo, J., Jiao,  
594 X., Yeow, W.-S., Katiyar, S., *et al.* (2010). The canonical NF-kappaB pathway governs  
595 mammary tumorigenesis in transgenic mice and tumor stem cell expansion. *Cancer research* 70,  
596 10464-10473.
- 597 López, Á.G., Seoane, J.M., and Sanjuán, M.A.F. (2017). Dynamics of the cell-mediated immune  
598 response to tumour growth. *Phil Trans R Soc A* 375, 20160291-20160214.

- 599 Lu, P., Weaver, V.M., and Werb, Z. (2012). The extracellular matrix: A dynamic niche in cancer  
600 progression. *J Cell Biol* *196*, 395-406.
- 601 Lu, X., Mu, E., Wei, Y., Riethdorf, S., Yang, Q., Yuan, M., Yan, J., Hua, Y., Tiede, B.J., Lu, X.,  
602 *et al.* (2011). VCAM-1 Promotes Osteolytic Expansion of Indolent Bone Micrometastasis of  
603 Breast Cancer by Engaging  $\alpha 4\beta 1$ -Positive Osteoclast Progenitors. *Cancer cell* *20*, 701-714.
- 604 Mabe, N.W., Fox, D.B., Lupo, R., Decker, A.E., Phelps, S.N., Thompson, J.W., and Alvarez,  
605 J.V. (2018). Epigenetic silencing of tumor suppressor Par-4 promotes chemoresistance in  
606 recurrent breast cancer. *The Journal of clinical investigation* *128*, 4413-4428.
- 607 Meads, M.B., Gatenby, R.A., and Dalton, W.S. (2009). Environment-mediated drug resistance: a  
608 major contributor to minimal residual disease. *Nature Reviews Cancer* *9*, 665.
- 609 Moody, S.E. (2002). Conditional activation of Neu in the mammary epithelium of transgenic  
610 mice results in reversible pulmonary metastasis. *Cancer cell* *2*, 451-461.
- 611 Neville-Webbe, H.L., Cross, N.A., Eaton, C.L., Nyambo, R., Evans, C.A., Coleman, R.E., and  
612 Holen, I. (2004). Osteoprotegerin (OPG) produced by bone marrow stromal cells protects breast  
613 cancer cells from TRAIL-induced apoptosis. *Breast cancer research and treatment* *86*, 269-279.
- 614 Pollard, J.W. (2004). Opinion: Tumour-educated macrophages promote tumour progression and  
615 metastasis. *Nature Reviews Cancer* *4*, 71-78.
- 616 Provenzano, P.P., Inman, D.R., Eliceiri, K.W., Knittel, J.G., Yan, L., Rueden, C.T., White, J.G.,  
617 and Keely, P.J. (2008). Collagen density promotes mammary tumor initiation and progression.  
618 *BMC Medicine* *6*, 11.
- 619 Santa-Cecília, F.V., Socias, B., Ouidja, M.O., Sepulveda-Diaz, J.E., Acuña, L., Silva, R.L.,  
620 Michel, P.P., Del-Bel, E., Cunha, T.M., and Raisman-Vozari, R. (2016). Doxycycline Suppresses  
621 Microglial Activation by Inhibiting the p38 MAPK and NF- $\kappa$ B Signaling Pathways.  
622 *Neurotoxicity Research* *29*, 447-459.
- 623 Schindelin, J., Arganda-Carreras, I., Frise, E., Kaynig, V., Longair, M., Pietzsch, T., Preibisch,  
624 S., Rueden, C., Saalfeld, S., Schmid, B., *et al.* (2012). Fiji: an open-source platform for  
625 biological-image analysis. *Nature methods* *9*, 676-682.
- 626 Sequist, L.V., Waltman, B.A., Dias-Santagata, D., Digumarthy, S., Turke, A.B., Fidias, P.,  
627 Bergethon, K., Shaw, A.T., Gettinger, S., Cospers, A.K., *et al.* (2011). Genotypic and histological  
628 evolution of lung cancers acquiring resistance to EGFR inhibitors. *Science translational medicine*  
629 *3*, 75ra26-75ra26.
- 630 Sharma, S.V., Lee, D.Y., Li, B., Quinlan, M.P., Takahashi, F., Maheswaran, S., McDermott, U.,  
631 Azizian, N., Zou, L., Fischbach, M.A., *et al.* (2010). A Chromatin-Mediated Reversible Drug-  
632 Tolerant State in Cancer Cell Subpopulations. *Cell* *141*, 69-80.
- 633 Soria, G., and Ben-Baruch, A. (2008). The inflammatory chemokines CCL2 and CCL5 in breast  
634 cancer. *Cancer letters* *267*, 271-285.

- 635 Sosa, M.S., Avivar-Valderas, A., Bragado, P., Wen, H.-C., and Aguirre-Ghiso, J.A. (2011).  
636 ERK1/2 and p38 $\alpha$ / $\beta$  Signaling in Tumor Cell Quiescence: Opportunities to Control Dormant  
637 Residual Disease. *Clinical Cancer Research* 17, 5850-5857.
- 638 Strachan, D.C., Ruffell, B., Oei, Y., Bissell, M.J., Coussens, L.M., Pryer, N., and Daniel, D.  
639 (2014). CSF1R inhibition delays cervical and mammary tumor growth in murine models by  
640 attenuating the turnover of tumor-associated macrophages and enhancing infiltration by CD8 +T  
641 cells. *Oncoimmunology* 2, e26968-26913.
- 642 Subramanian, A., Tamayo, P., Mootha, V.K., Mukherjee, S., Ebert, B.L., Gillette, M.A.,  
643 Paulovich, A., Pomeroy, S.L., Golub, T.R., Lander, E.S., *et al.* (2005). Gene set enrichment  
644 analysis: a knowledge-based approach for interpreting genome-wide expression profiles.  
645 *Proceedings of the National Academy of Sciences of the United States of America* 102, 15545-  
646 15550.
- 647 Team, R.C. (2013). R: A language and environment for statistical computing. . R Foundation for  
648 Statistical Computing, Vienna, Austria.
- 649 Tempfer, C. (2011). Basal-like molecular subtype and HER4 up-regulation and response to  
650 neoadjuvant chemotherapy in breast cancer. *Oncology reports*.
- 651 Thannickal, V.J. (2012). Mechanisms of pulmonary fibrosis: role of activated myofibroblasts and  
652 NADPH oxidase. *Fibrogenesis & tissue repair* 5, S23-S23.
- 653 Velasco-Velazquez, M., Jiao, X., De La Fuente, M., Pestell, T.G., Ertel, A., Lisanti, M.P., and  
654 Pestell, R.G. (2012). CCR5 Antagonist Blocks Metastasis of Basal Breast Cancer Cells. *Cancer*  
655 *research* 72, 3839-3850.
- 656 Zhu, Y., Knolhoff, B.L., Meyer, M.A., Nywening, T.M., West, B.L., Luo, J., Wang-Gillam, A.,  
657 Goedegebuure, S.P., Linehan, D.C., and DeNardo, D.G. (2014). CSF1/CSF1R Blockade  
658 Reprograms Tumor-Infiltrating Macrophages and Improves Response to T-cell Checkpoint  
659 Immunotherapy in Pancreatic Cancer Models. *Cancer research* 74, 5057-5069.  
660
- 661

662 **Figure Legends**

663

664 **Figure 1) Her2 downregulation induces an inflammatory gene expression program driven**  
665 **by the TNF $\alpha$ /IKK pathway. (a)** RNA-seq analysis of two independent primary Her2-driven  
666 tumor cell lines in the presence of Her2 expression (+dox) or two days following Her2  
667 downregulation (-dox). The heatmap shows the top 100 differentially expressed genes between  
668 +dox and -dox conditions. R1 and R2 are biological replicates. **(b)** Gene set enrichment analysis  
669 (GSEA) of RNA-seq data showing enrichment of an inflammatory response signature and a  
670 TNF $\alpha$ /NF- $\kappa$ B signature in cells following Her2 downregulation. P-values and normalized  
671 enrichment scores (NES) are shown. **(c)** Heatmap showing expression of select genes from the  
672 TNF $\alpha$ /NF- $\kappa$ B signature in the presence of Her2 expression (+dox) or following Her2 deinduction  
673 (-dox). **(d)** qRT-PCR analysis of CCL5 expression following 1 or 2-day treatment with conditioned  
674 media harvested from primary cells following Her2 downregulation. Dox was added to  
675 conditioned media prior to treatment to maintain Her2 expression in target cells. Results shown  
676 are representative of two independent experiments. **(e)** qRT-PCR of TNF $\alpha$  expression in primary  
677 cells in the presence of Her2 expression (+dox) or 2 and 4 days following Her2 downregulation.  
678 Results shown are representative of two independent experiments. **(f)** Primary tumor cells were  
679 treated with conditioned media as described in (d), and activation of the NF- $\kappa$ B pathway was  
680 assessed by Western blot analysis of total and phospho-p65. Results show 3 biological replicates  
681 per time point. **(g)** qRT-PCR analysis of the indicated genes in primary tumor cells in the presence  
682 of Her2 expression (+dox) or 1 and 2 days following Her2 downregulation (-dox). At the time of  
683 Her2 downregulation, cells were treated with the pan-IKK inhibitor IKK16 (100 nM) or vehicle  
684 control. Results show the average of 3 biological replicates per condition.

685 Error bars denote mean  $\pm$  SEM. Significance was determined using a two-tailed Student's t-test.

686

687 **Figure 1 – figure supplement 1** (a) qRT-PCR analysis of Erbb2 expression in primary cells with  
688 Her2 on (+dox) or Her2 off (-dox). (b) Gene set enrichment analysis (GSEA) of RNA-seq data  
689 showing an E2F gene signature is enriched in cells with Her2 signaling on. P-values and  
690 normalized enrichment scores (NES) are shown. (c) Western blot showing p65 phosphorylation in  
691 primary tumor cells treated with the indicated concentration of Neratinib for 24 hours, or 24 hours  
692 following dox withdrawal. (d-f) qRT-PCR analysis of TNF $\alpha$ , CCL5, and CXCL5 expression 24  
693 hours after treatment with 0.1  $\mu$ M Neratinib. (g) qRT-PCR analysis of CCL2, CCL5, and CXCL5  
694 expression in NIH-3T3 treated with 2  $\mu$ g/mL dox, 10 ng/mL TNF $\alpha$ , or both for 24 hours. (h) qRT-  
695 PCR analysis of Erbb2 expression of cells treated with -dox conditioned media with dox  
696 supplementation. (i) Primary tumor cells were treated with +dox conditioned media and activation  
697 of the NF- $\kappa$ B pathway was assessed by Western blot analysis of total and phospho-p65. Results  
698 show 2 biological replicates per time point.

699

700 **Figure 2) Immune cell infiltration during tumor regression and residual disease.** (a) H&E-  
701 stained section of a representative residual tumor from a previously tumor-bearing MTB/TAN  
702 mouse. Insets show higher-magnification view of residual tumor cells (left) and staining for CK8  
703 (right). (b-d) Representative images of a primary tumor (b), regressing tumor (5 days -dox) (c),  
704 and residual tumor (d), stained with H&E, Masson's Trichome (MT), CD45, or F4/80. Primary  
705 tumors show little collagen deposition and only modest leukocyte infiltration. Her2  
706 downregulation leads to infiltration of CD45+ cells, predominantly F4/80+ macrophages. Residual  
707 tumors have abundant collagen deposition and leukocyte infiltration.

708

709 **Figure 2 – figure supplement 1** (a) CD3 staining of representative MTB;TAN primary, 5 days -  
710 dox, and residual tumors. (b) Bright-field and fluorescent images of a representative GFP-labeled  
711 orthotopic residual tumor in the context of a non-fluorescent mammary gland. (c) Quantification  
712 of IHC and MT staining of primary, regressing, and residual tumors from the MTB;TAN model.  
713 (d-f) F4/80 staining of representative orthotopic primary, 5 days -dox, and residual tumors showing  
714 macrophage infiltration.

715

716 **Figure 3) Differential cytokine expression in residual tumors.** (a) Volcano plot showing  
717 differential cytokine expression between primary and residual tumors. Antibody-based cytokine  
718 arrays were used to measure cytokine expression in orthotopic primary tumors or microdissected  
719 residual tumors. Cytokines that are upregulated (fold change >2, p-value <0.1) in dormant tumors  
720 are in red, and downregulated cytokines (fold change <-2, p-value <0.1) are in blue. Significance  
721 was determined using a two-tailed Student's t-test. (b) Quantification of CCL5, IL-13, IGFBP6,  
722 VCAM-1, OPG, HGF, Resistin, and P-Selectin expression in primary tumors and residual tumors.  
723 Values were derived from the cytokine arrays shown in (a). Significance was determined using a  
724 two-tailed Student's t-test. (c) CCL5 expression in 18 matched pre- and post-treatment samples  
725 from GSE10281. Red lines show tumors in which CCL5 expression increased following treatment  
726 (>1.5-fold change), and blue lines show tumors with decreased CCL5 expression (<1.5-fold  
727 change). (d) Average CCL5 expression in pre- and post-treatment samples from (e). Significance  
728 was determined using a two-tailed paired Student's t-test.

729 Error bars denote mean  $\pm$  SEM.

730



731 **Figure 3 – figure supplement 1)** (a) Heatmap showing expression of selected cytokine and  
732 chemokine genes from 18 matched human breast tumors prior to treatment, or in residual tumors  
733 following neoadjuvant Letrozole treatment (GSE10281). Gene expression values were log2  
734 transformed and median centered. (b-m) Average expression of CCL2, CXCL1, CXCL2, CXCL5,  
735 SELE, HGF, IGFBP6, IL-13, TNFRSF11B, SELP, RETN, and VCAM-1 in 18 matched pre- and  
736 post-treatment samples following neoadjuvant Letrozole treatment (GSE10281). Two-tailed  
737 paired t-test was performed between pre- and post-treatment samples. (n) Average CCL5  
738 expression in 25 matched pre- and post-treatment samples from human breast tumors treated with  
739 neoadjuvant chemotherapy (GSE21974). Two-tailed paired t-test was performed between pre- and  
740 post-treatment samples.

741  
742 **Figure 3 – source data)** Cytokine array expression data analysis from arrays Q1 and Q4.

743  
744 **Figure 4) CCL5 expression promotes tumor recurrence following Her2 downregulation. (a)**  
745 CCL5 protein levels in orthotopic primary (n=4), residual (n=3), and recurrent (n=2) tumors as  
746 determined by ELISA. **(b)** CCL5 protein levels in primary tumor cells engineered to express  
747 CCL5. Results show the mean  $\pm$  SEM for two independent experiments. Significance was  
748 determined using a two-tailed Student's t-test. **(c)** Recurrence-free survival for mice with control  
749 tumors or tumors expressing CCL5. CCL5 expression significantly accelerated recurrence  
750 (Hazards Ratio (HR) = 2.1, p = 0.02). Results are from a single experiment with 20 control tumors  
751 and 21 CCL5 tumors. P-values and hazards ratios are indicated. Statistical significance was  
752 determined by Mantel-Cox log rank test. **(d)** CCL5 expression as determined by ELISA in primary  
753 tumor cells expressing a control sgRNA or a sgRNA targeting CCL5. Results show the mean  $\pm$

754 SEM for a single representative experiment. **(e)** Recurrence-free survival of mice with control  
755 tumors or CCL5 knockout tumors. CCL5 knockout in tumor cells did not significantly delay tumor  
756 recurrence (HR =0.76, p = 0.46). Results are from a single experiment with 26 control tumors  
757 (sgControl) and 24 sgCCL5 tumors. Statistical significance was determined by Mantel-Cox log  
758 rank test.

759

760 Error bars denote mean  $\pm$  SEM.

761

762 **Figure 5) CCL5 promotes macrophage infiltration in residual tumors. (a-d)** Flow cytometry  
763 of immune cells in primary (n=6), regressing (5 days -dox; n=3), residual (n=3), and recurrent  
764 (n=3) tumors from autochthonous MTB;TAN mice. Immune cell populations analyzed include  
765 CD11b+/F4/80+ macrophages (a), CD4+ T cells (b), CD8+ T cells (c), PDGFR $\alpha$  fibroblasts (d),  
766 and tumor cells (e). Each immune cell population was divided into CCR5- or CCR5+ cells, and  
767 the median fluorescence intensity (MFI) of the CCR5+ population was calculated. **(f)** Flow  
768 cytometry of CD45-/PDGFR $\alpha$ + fibroblasts in control residual tumors (n=4) or residual tumors  
769 expressing CCL5 (n=4). **(g)** Flow cytometry of CD11b+/F4/80+ macrophages in control residual  
770 tumors (n=4) or residual tumors expressing CCL5 (n=4).

771

772 Error bars denote mean  $\pm$  SEM. Significance was determined using a two-tailed Student's t-test. \*

773 p < 0.05, \*\* p < 0.01, \*\*\* p < 0.001, \*\*\*\* p < 0.0001

774

775 **Figure 5 - figure supplement 1)** (a) qRT-PCR analysis of Erbb2 in primary, 5 days – dox,  
776 residual, and recurrent tumors from the MTB;TAN model cohort used for flow cytometry analysis

777 of CCR5 expression. (b) qRT-PCR analysis of CCR5 on sorted tumor cells and macrophages from  
778 primary, 5 days -dox, residual, and recurrent tumors from the MTB;TAN model. (c) Flow plots of  
779 CD45-/PDGFR $\alpha$ + fibroblasts in control (n=4) and CCL5-expressing (n=4) residual tumors (d)  
780 Flow plots of CD11b+/F4/80+ macrophages in control (n=4) and CCL5-expressing (n=4) residual  
781 tumors.

782

783 **Figure 5 – figure supplement 2)** Histograms showing CCR5 staining in macrophages, PDGFR $\alpha$   
784 fibroblasts, CD4+ T cells, CD8+ T cells, and tumor cells from primary tumors (n=6), regressing  
785 tumors (5 days -dox; n=3), residual tumors (n=3), and recurrent tumors (n=3).

786

787 **Figure 6) Macrophages express collagen and collagen deposition factors.** (a) RNA-seq  
788 analysis of tumor associated macrophages from primary (n=3), regressing (5 days -dox; n=3), and  
789 recurrent (n=3) tumors. The heatmap shows differentially expressed genes ( $p < 0.01$ , Student's t-  
790 test) between primary and recurrent TAMs. (b) Heatmap showing expression of specific collagen  
791 genes from RNA-seq analysis in (a). (c) qRT-PCR analysis of COL5A1, ASPN, COL24A1, and  
792 PCOLCE expression in the cohort in (a) along with sorted macrophages from residual tumors. ND  
793 = not detected (d) qRT-PCR analysis of COL5A1, ASPN, COL24A1, and PCOLCE expression in  
794 unsorted MTB;TAN primary (n=5) and recurrent (n=5) tumors. (e) Masson's trichrome staining  
795 showing collagen deposition in primary (n=3), residual (n=3), and recurrent (n=3) tumors from the  
796 MTB;TAN model. Collagen is stained in blue, and higher collagen staining is present in residual  
797 and recurrent tumors. (f) Masson's trichrome staining in a subset of control and CCL5-expressing  
798 orthotopic recurrent tumors. The entire cohort of tumors is shown in Figure 6 – figure supplement  
799 1.

800

801 Error bars denote mean  $\pm$  SEM. Significance was determined using a two-tailed Student's t-test. \*

802  $p < 0.05$ , \*\*\*  $p < 0.001$ .

803

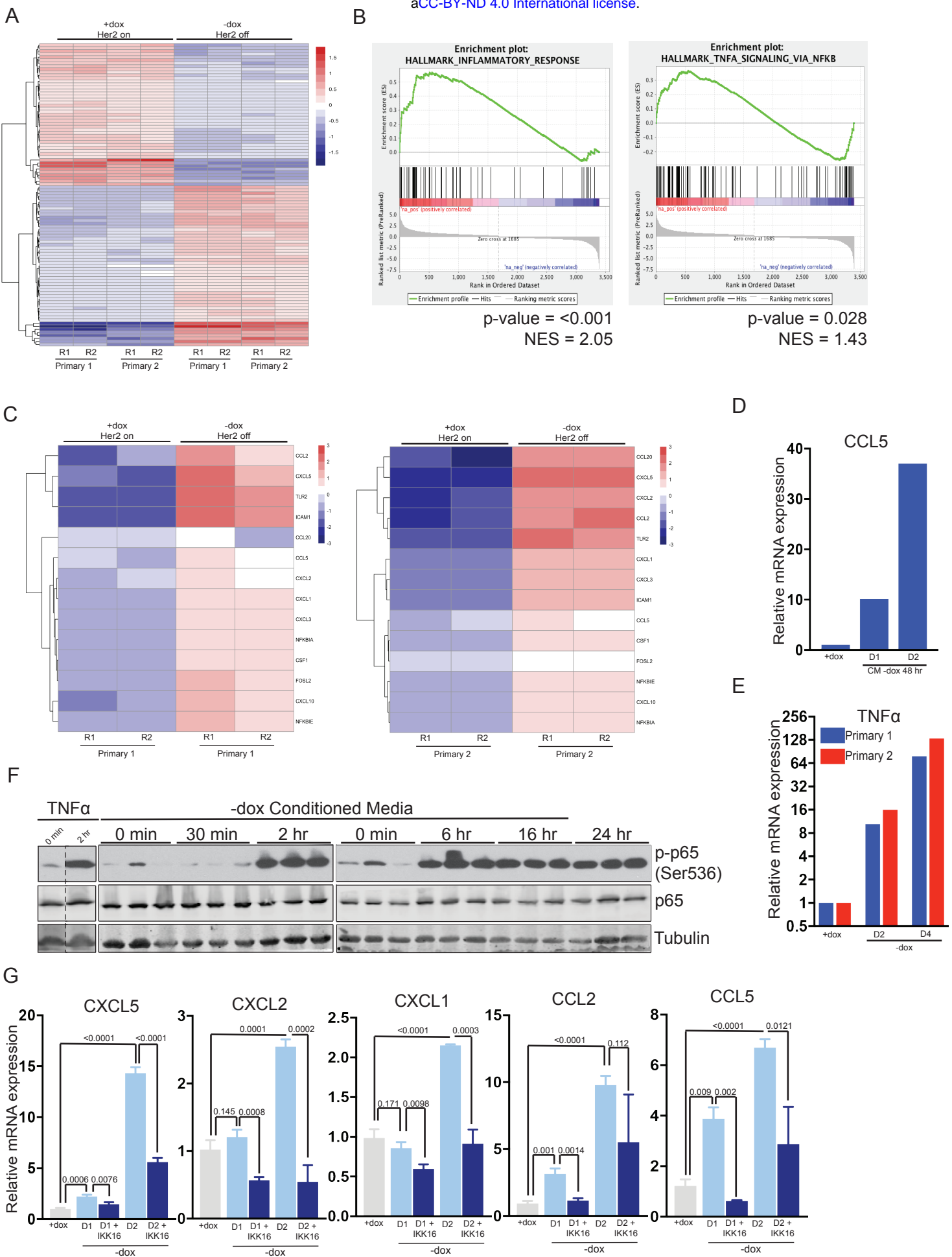
804 **Figure 6 – figure supplement 1)** (a) Average expression of ASPN, COL5A1, COL24A1, and  
805 PCOLCE in 18 matched pre- and post-treatment samples from human breast tumors treated with  
806 neoadjuvant Letrozole (GSE10281). Two-tailed paired t-test was performed between pre- and  
807 post-treatment samples. (b) Masson's trichrome staining showing collagen deposition in control  
808 (n=4) and CCL5-expressing (n=4) recurrent tumors. (c) Quantification of (b).

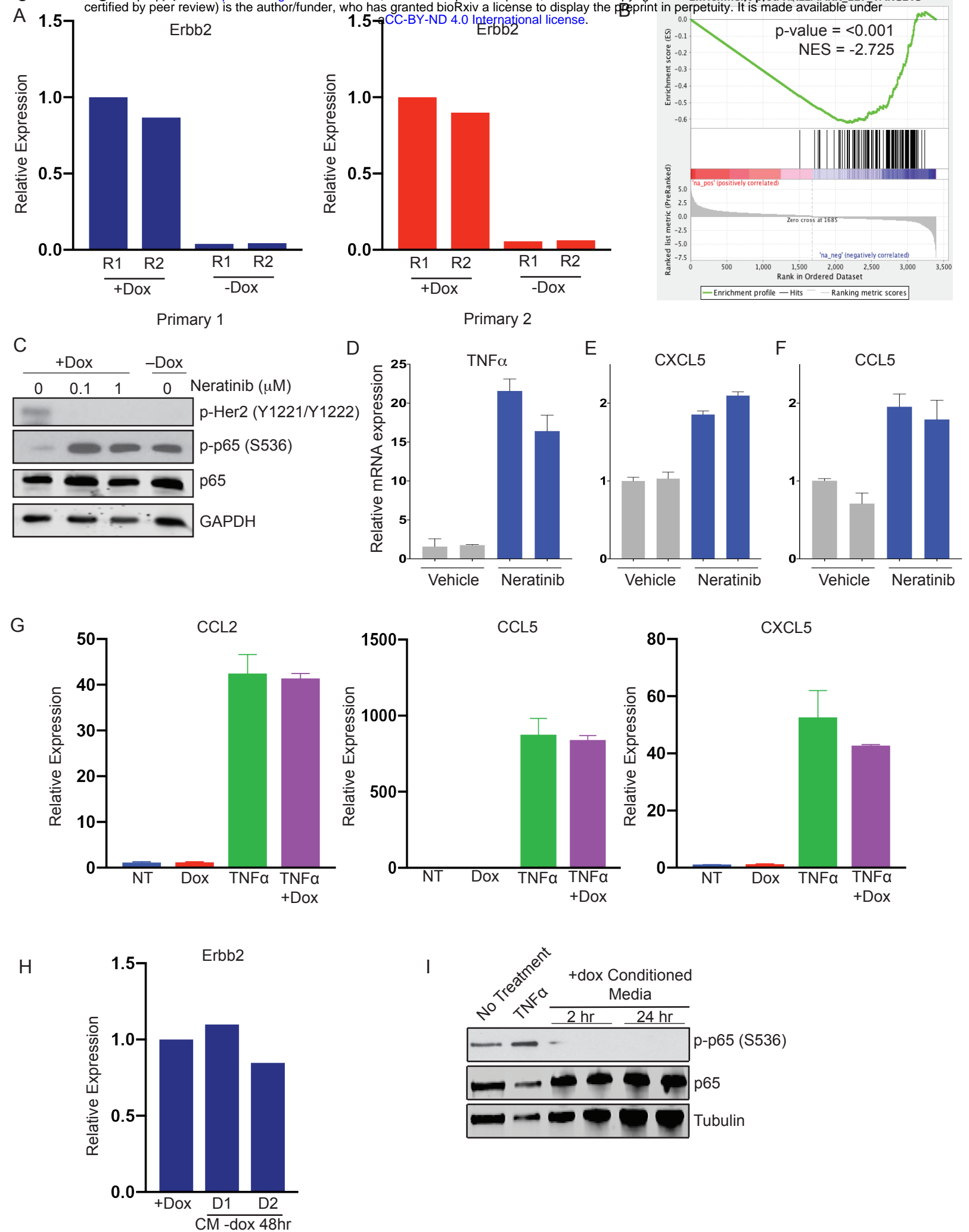
809

810 **Figure 6 – source data 1)** Differentially expressed genes from RNA-seq from primary and  
811 recurrent tumor cell lines used to clear contaminants from TAM RNA-seq

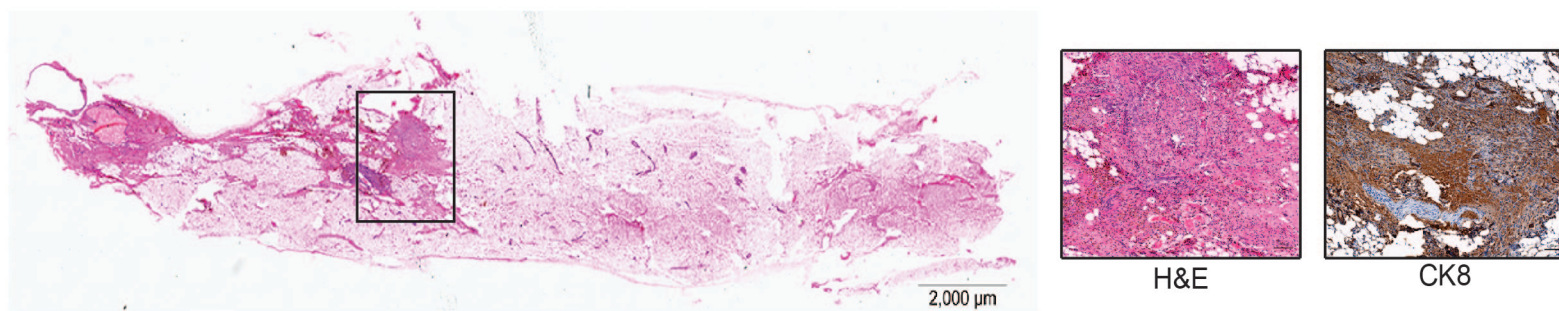
812 **Figure 6 – source data 2)** Candidate list of differentially expressed genes between primary and  
813 recurrent TAMs after filtering

814



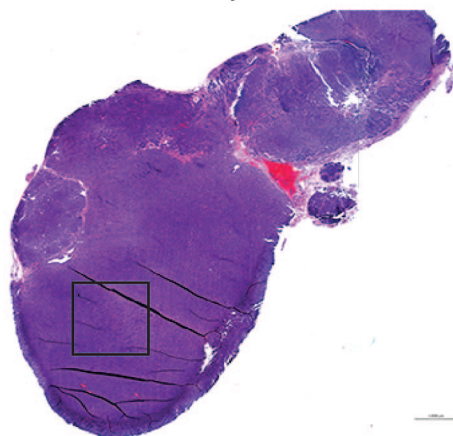


A



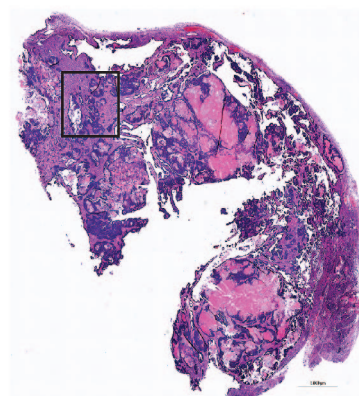
B

Primary Tumor



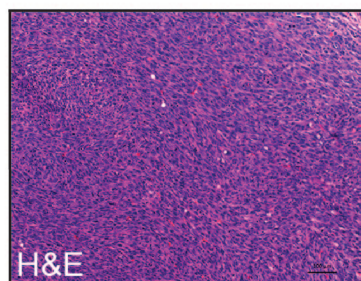
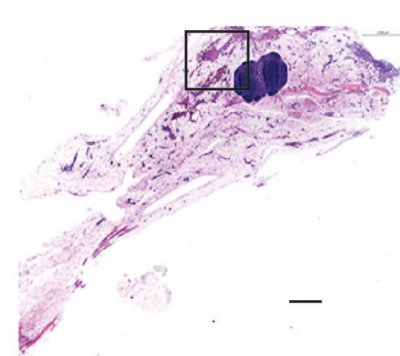
C

5 day -Dox

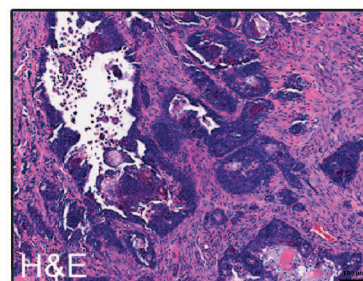


D

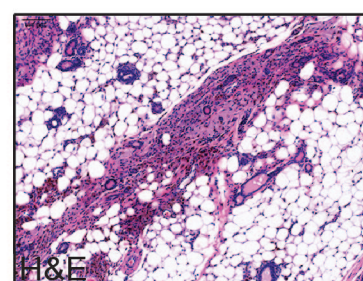
Residual Tumor



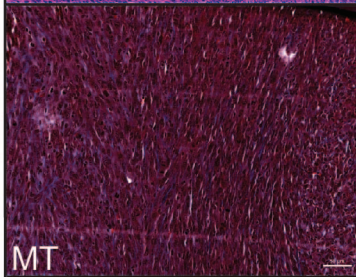
H&E



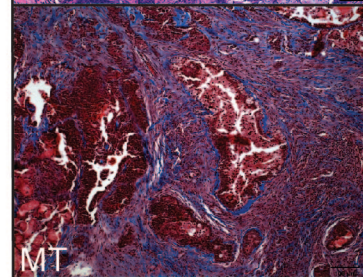
H&E



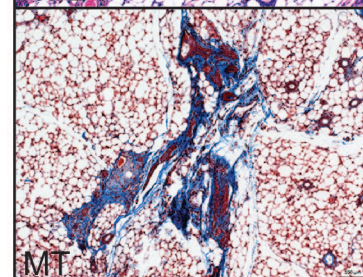
H&E



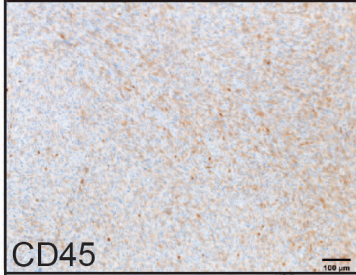
MT



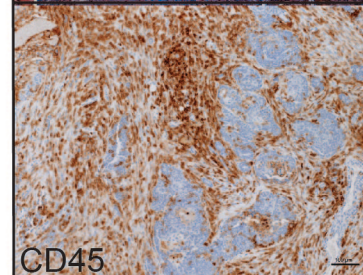
MT



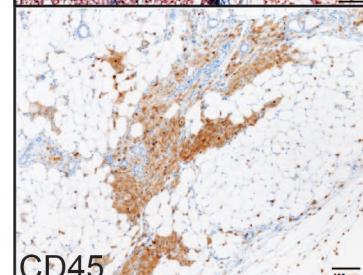
MT



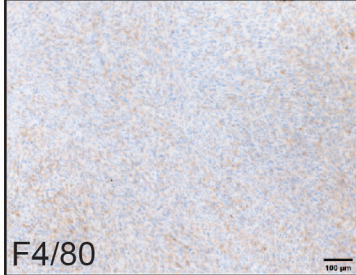
CD45



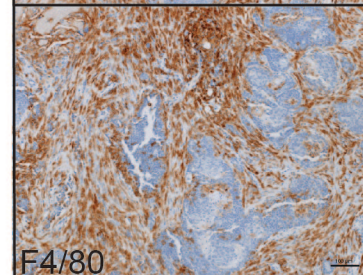
CD45



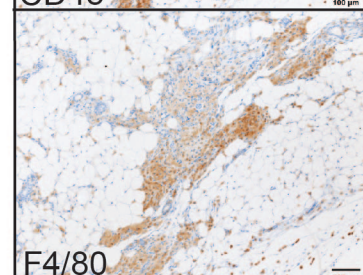
CD45



F4/80

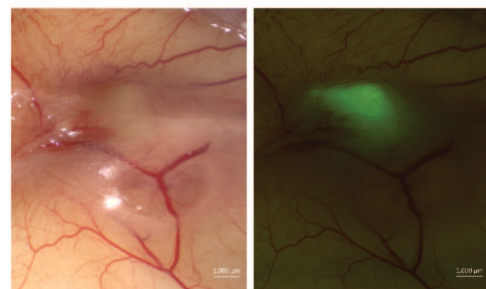
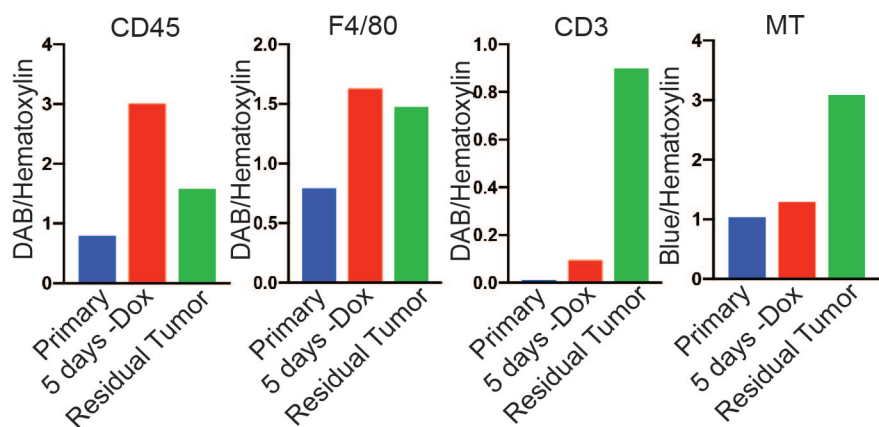


F4/80

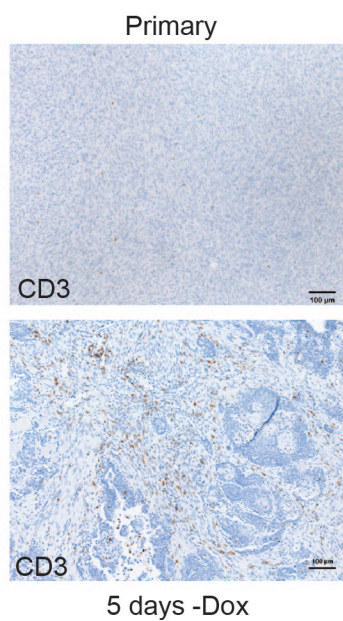


F4/80

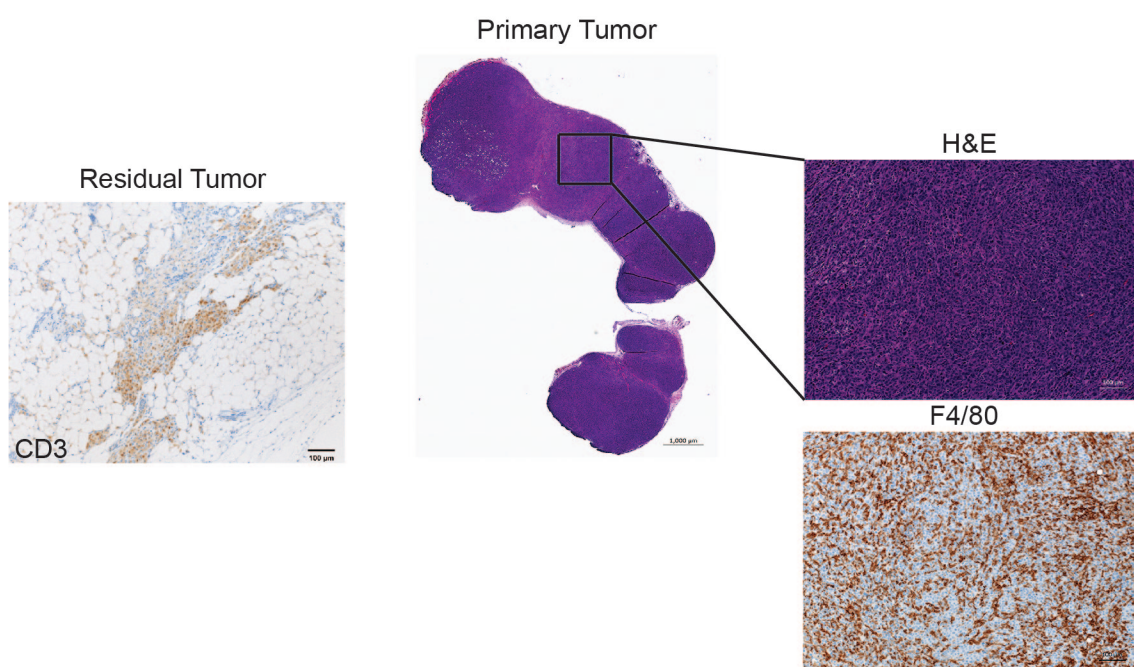
A



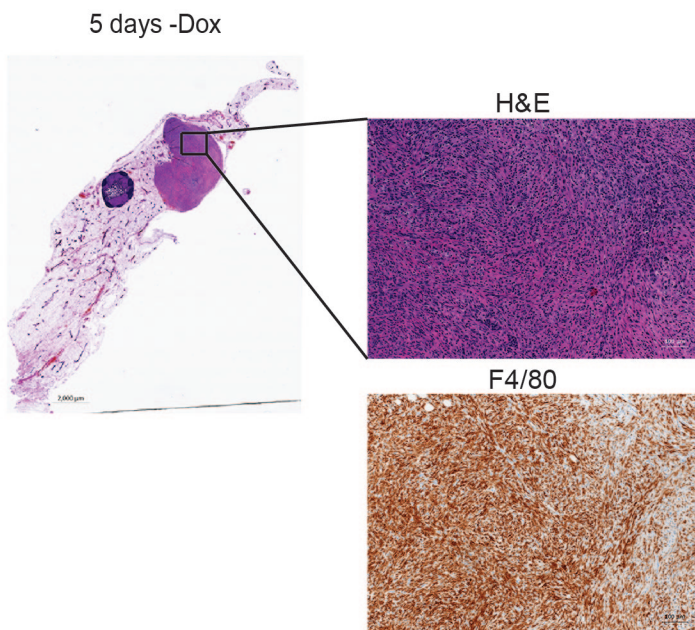
B



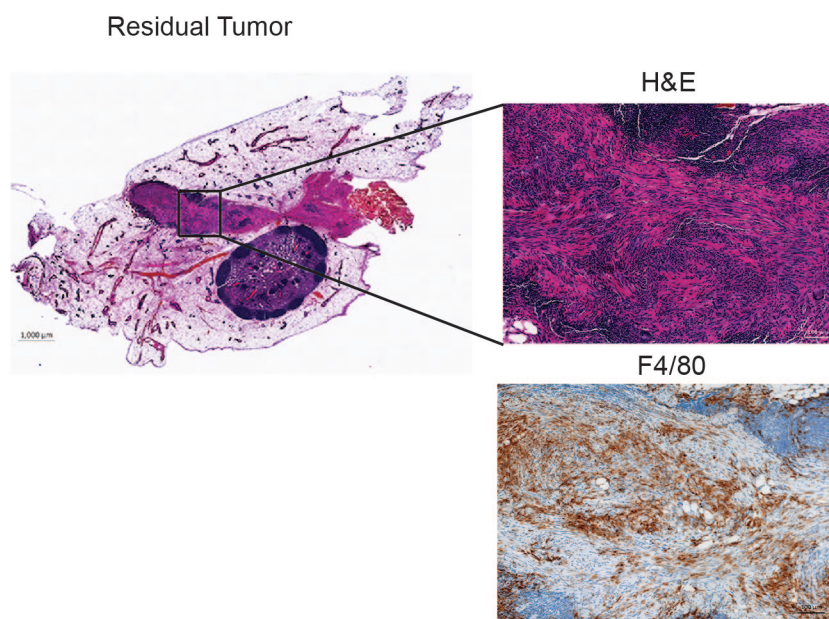
D



E

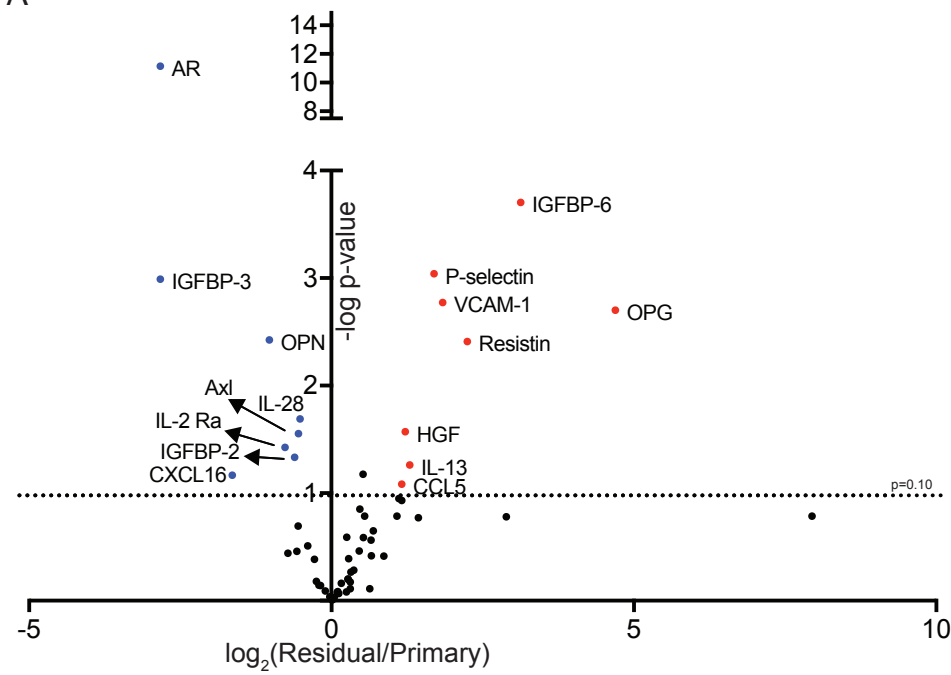


F

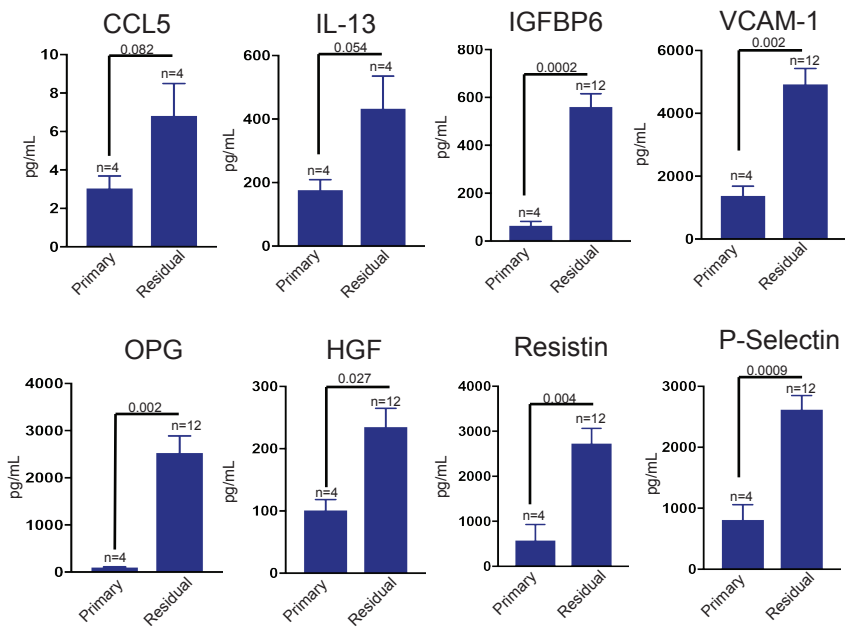




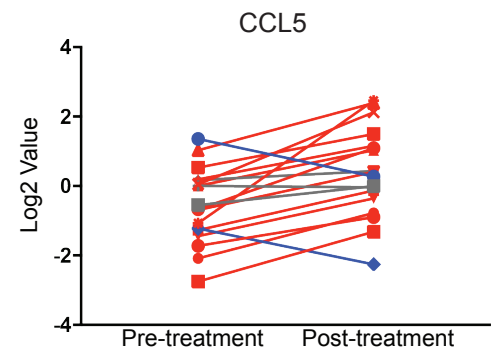
A



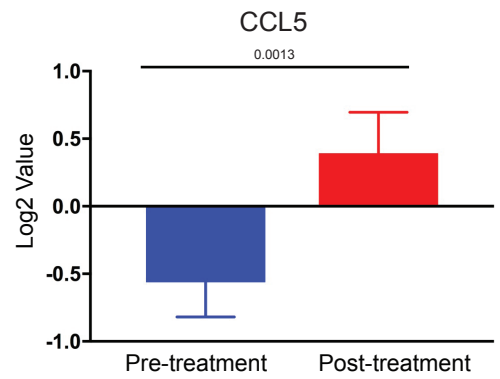
B

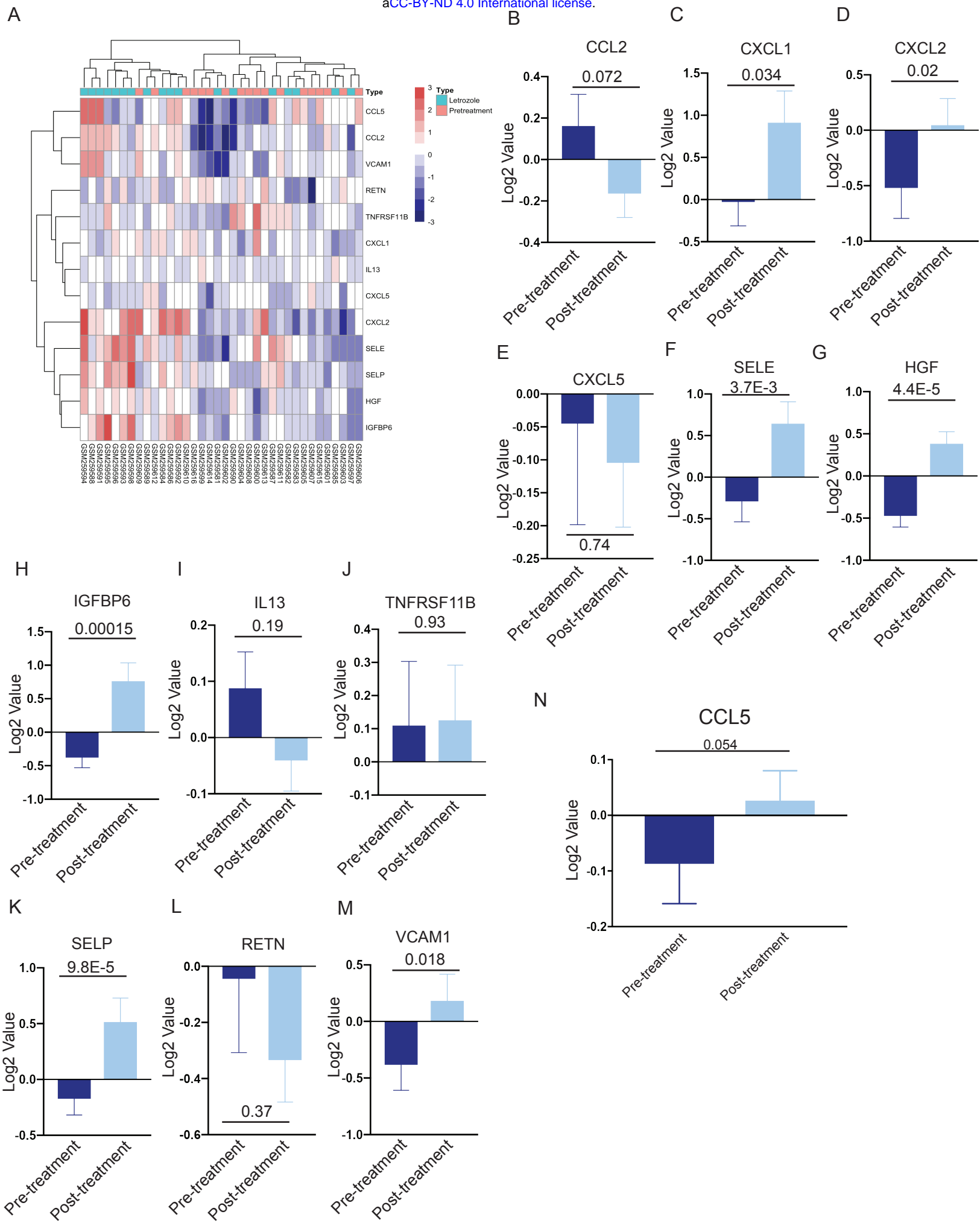


C

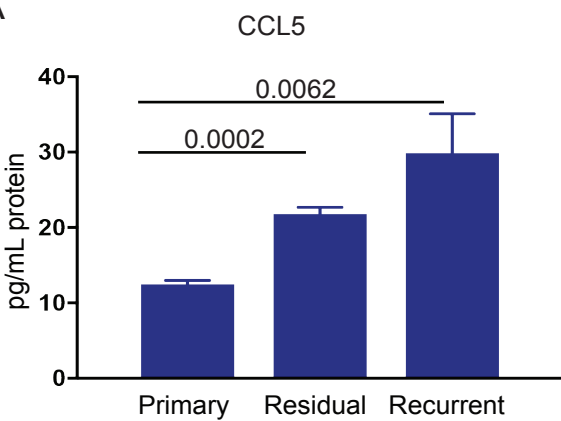


D

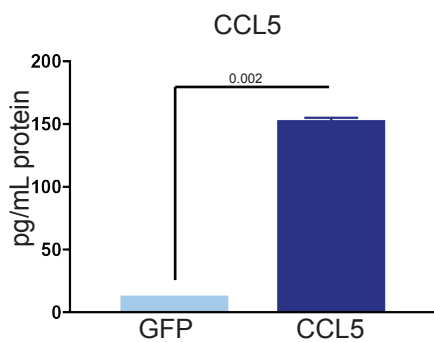




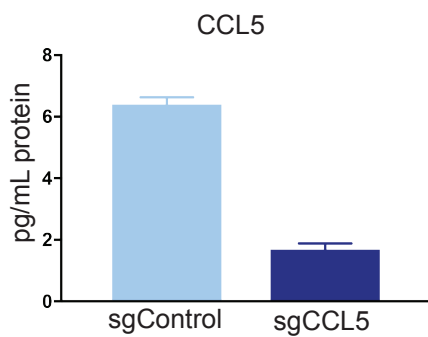
A



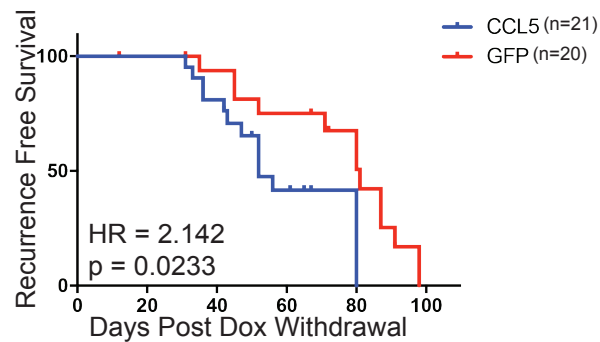
B



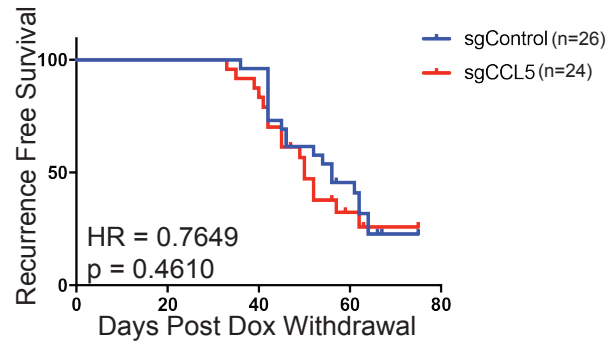
D

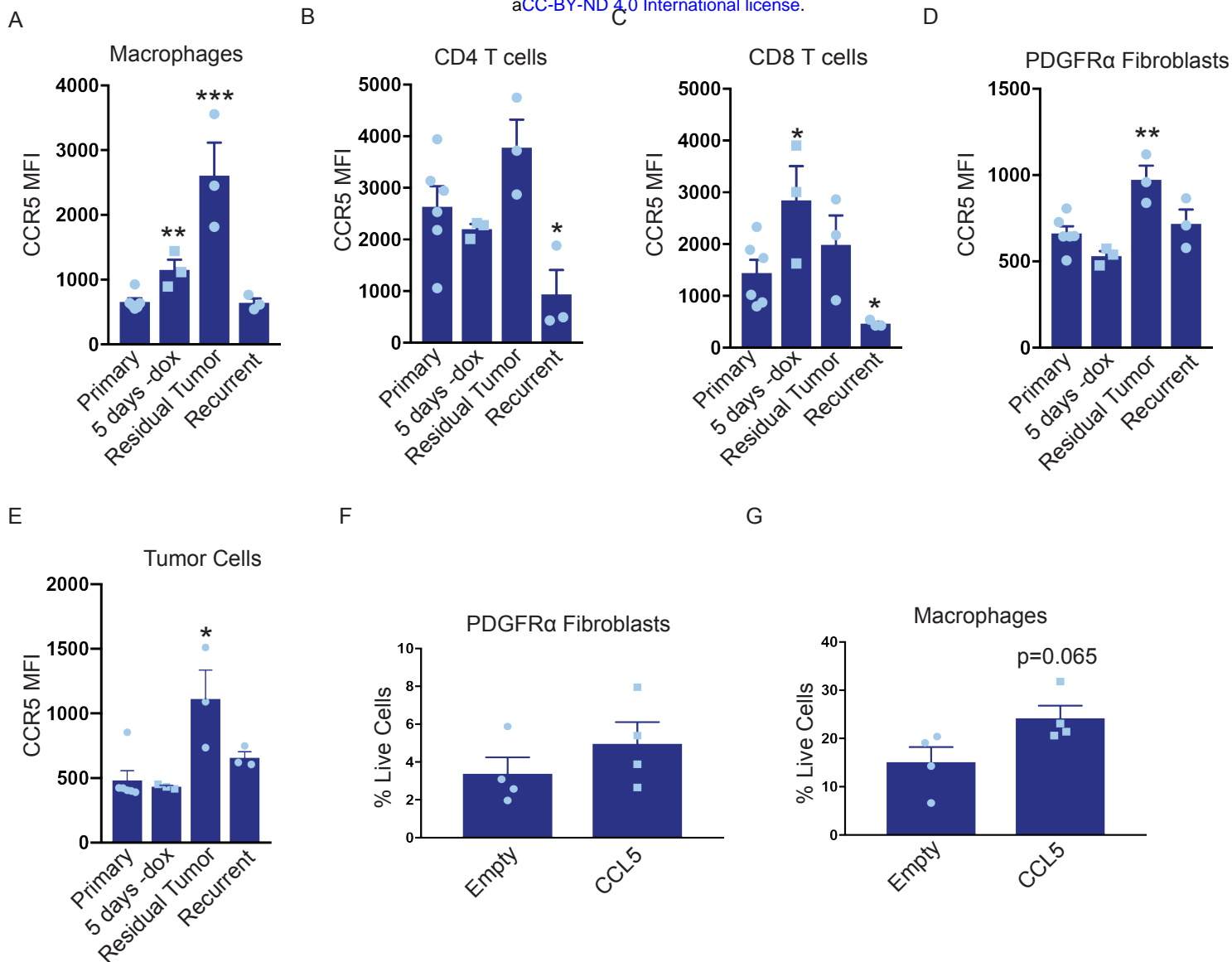


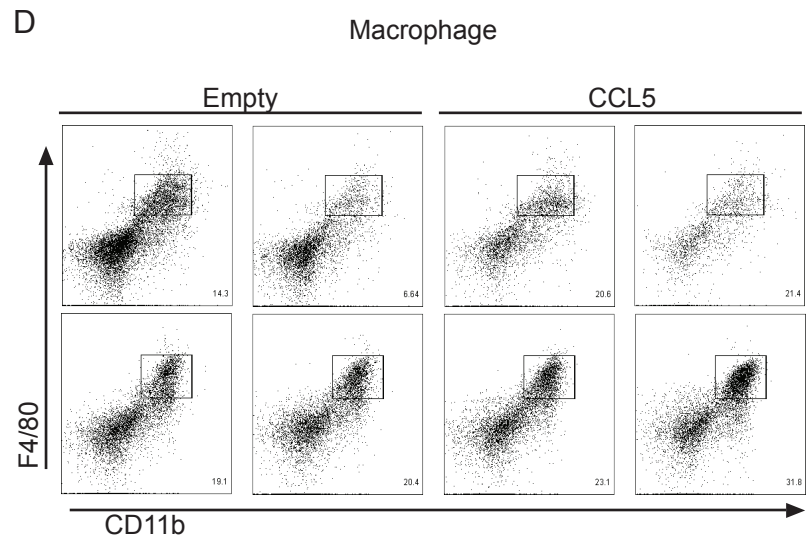
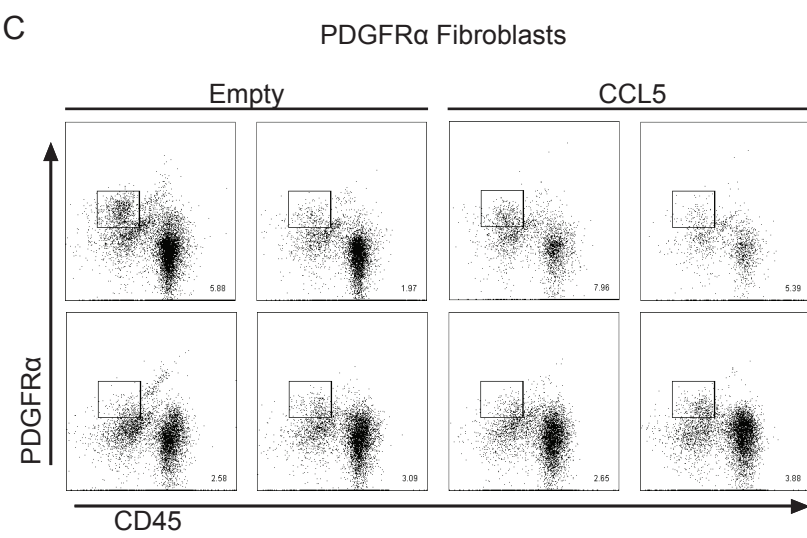
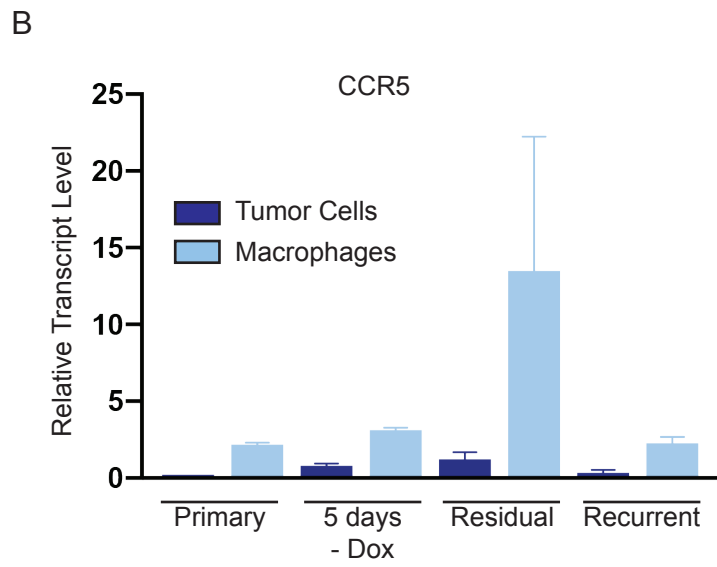
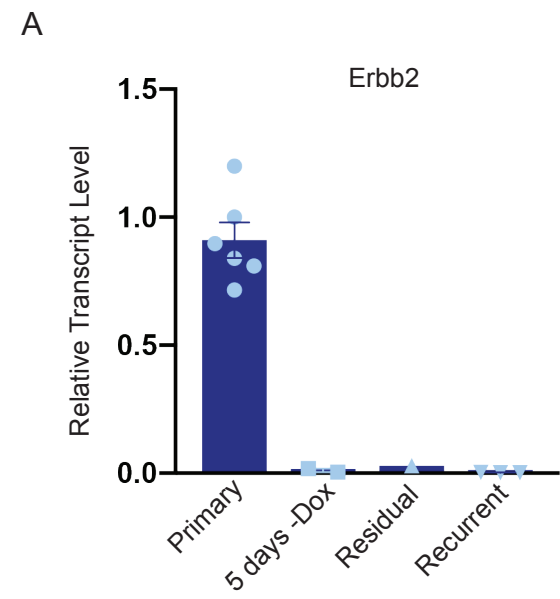
C

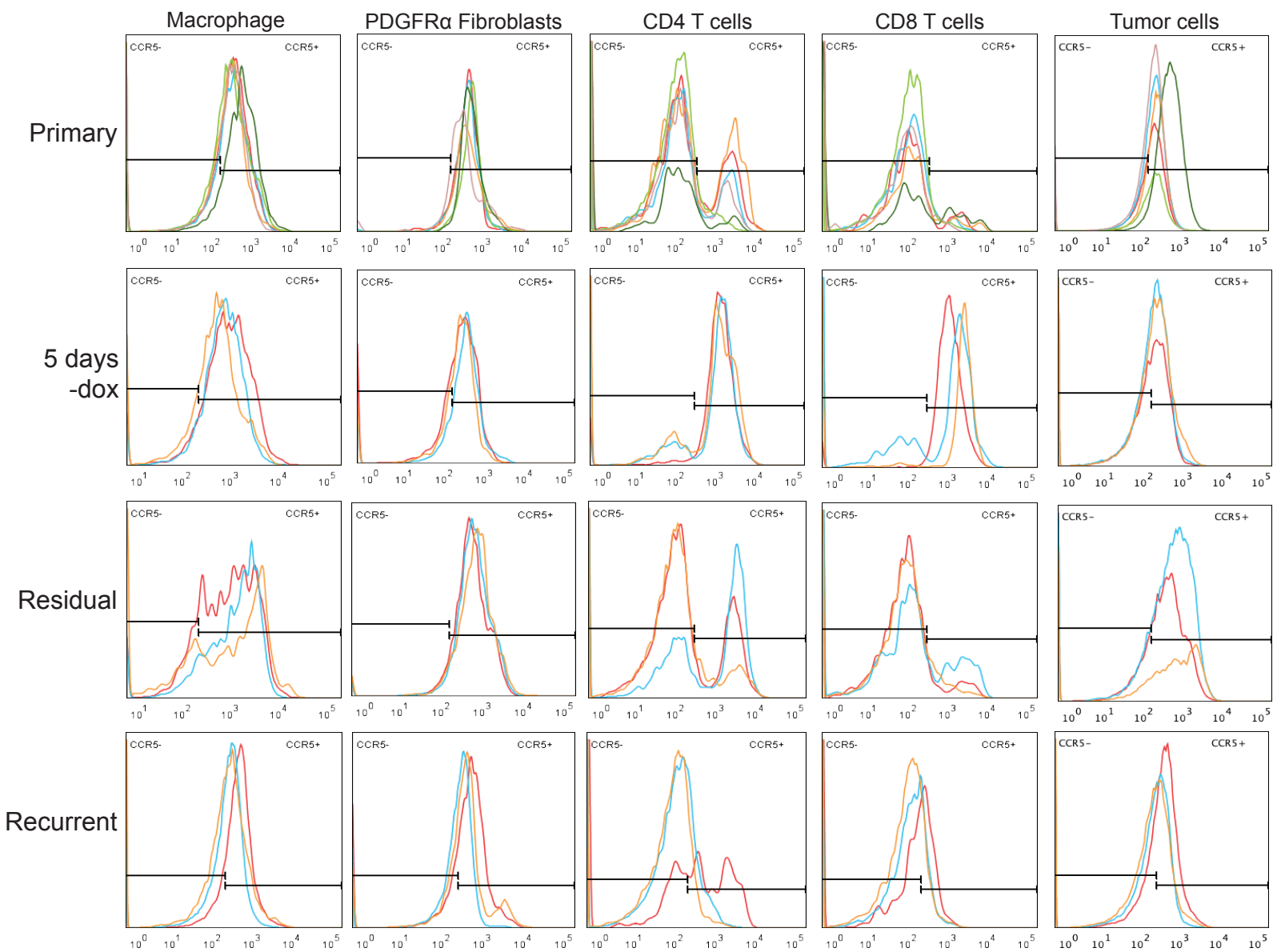


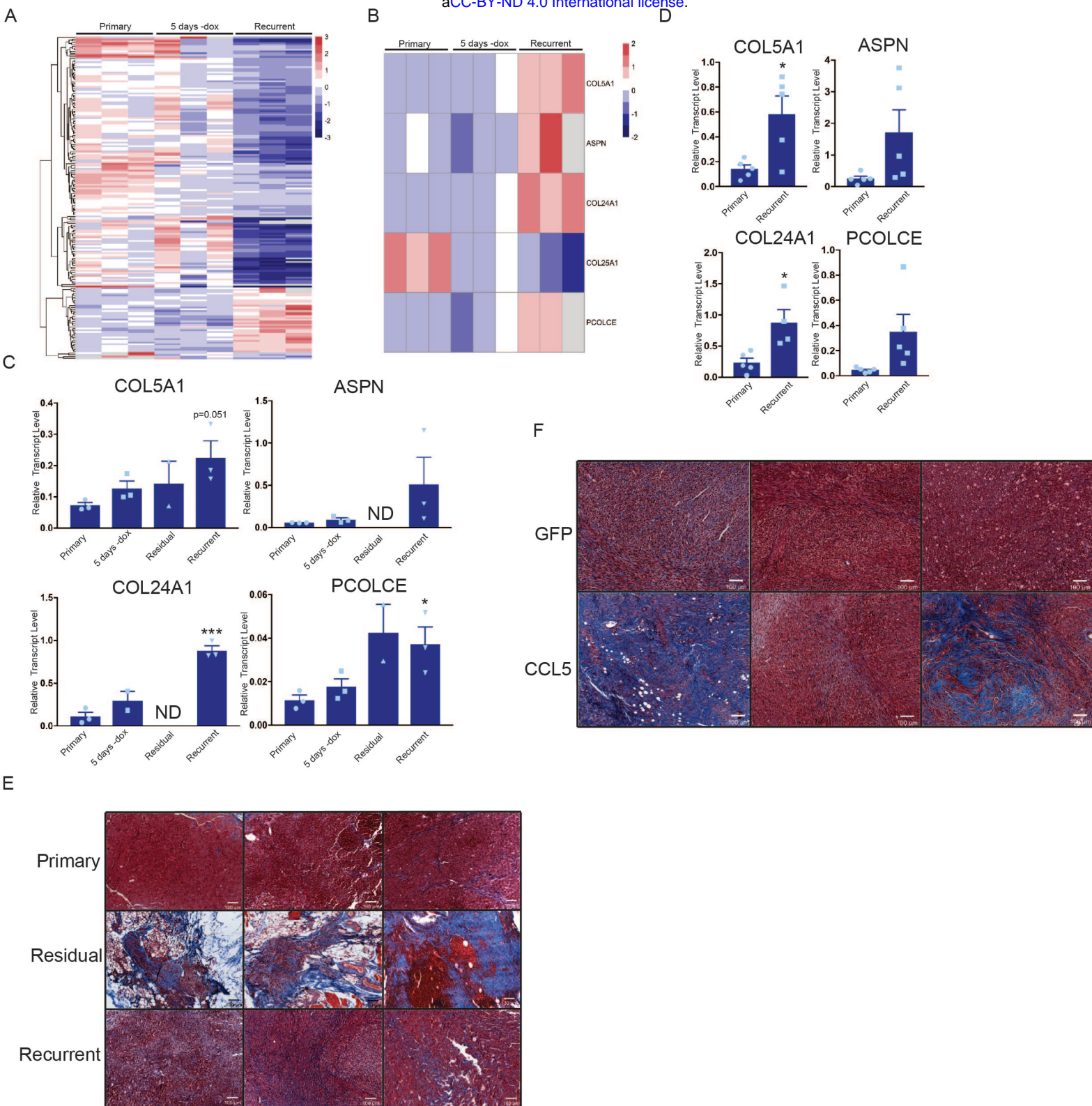
E



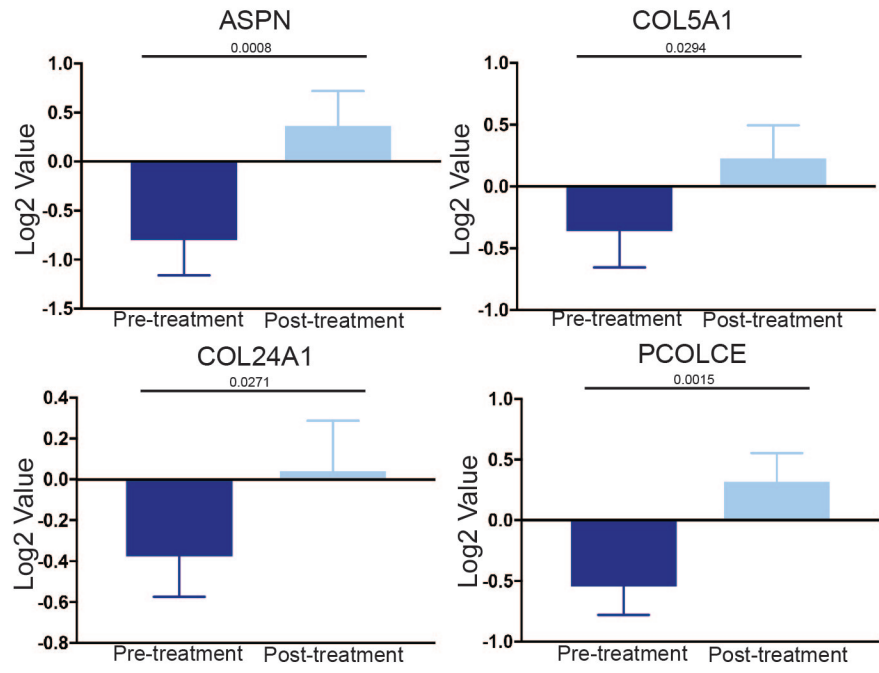




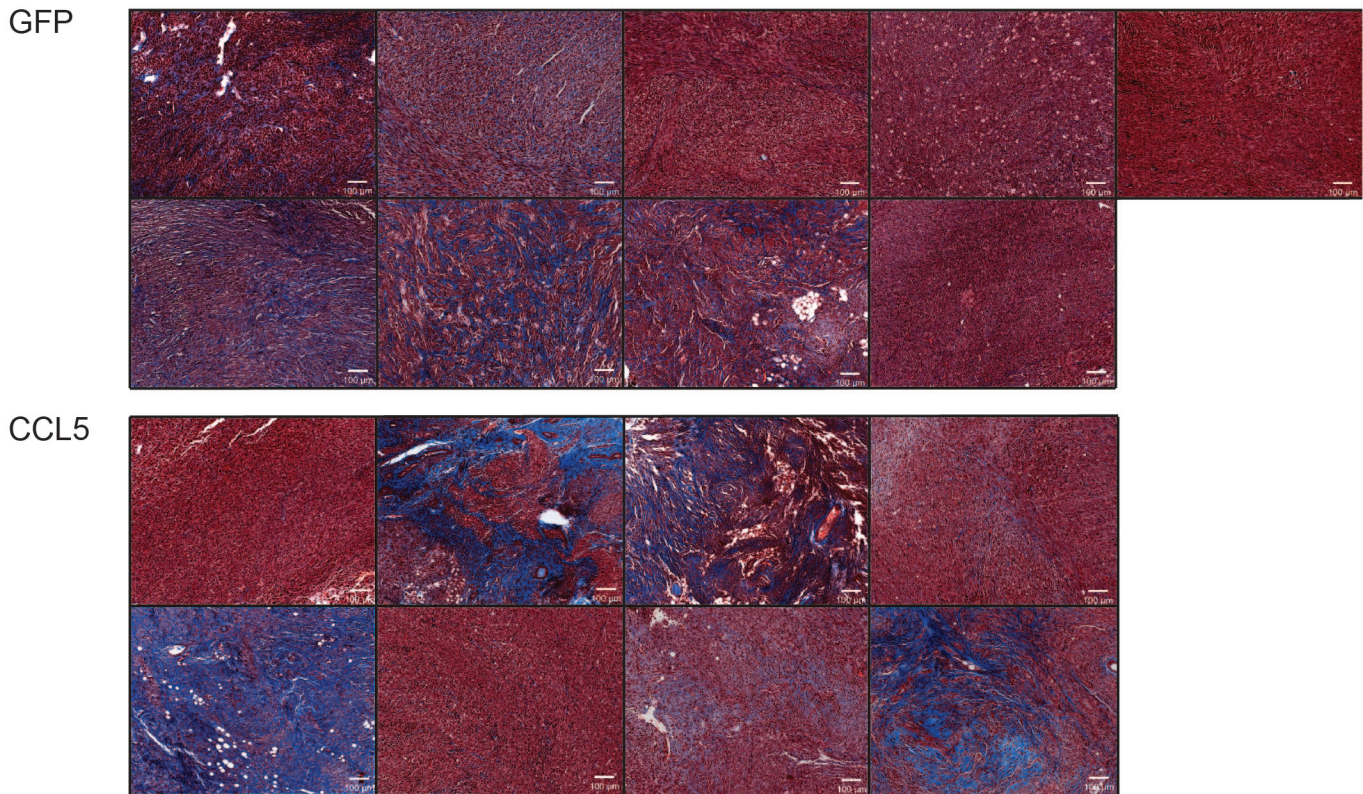




A



B



C

